Behaviour of cellular steel beams at ambient and high-temperature conditions

Sabrina Benyettou Oribi [a], Abdelhak Kada [b], Belkacem Lamri [b], Luis Mesquita [c],[*]

[a] LISICPE, LSGR, Faculty of Civil Engineering and Architecture, UHBC, Ouled Fares, BP. 78C, Chlef 02180, Algeria
[b] LISICPE, Faculty of Civil Engineering and Architecture, UHBC, Ouled Fares, BP. 78C, Chlef 02180, Algeria
[c] Institute for Sustainability and Innovation in Structural Engineering (ISISE), Polytechnic Institute of Bragança, Campus Santa Apolónia Ap. 1134, 5300-253 Bragança, Portugal

ABSTRACT

New developments in building construction have been observed to attain sustainable design criteria and the efficient use of raw materials, as steel is an example. This led to an increase in recent research on the optimization of geometric configurations of web-opening steel sections to meet cost-effectiveness in structural design. Improvement of the design method for perforated unrestrained steel beams to assess their behaviour under lateral torsional buckling (LTB) is still an ongoing issue for scientists and designers alike. In this article, cellular beams bound to instability were studied analytically by Eurocode and numerically by the finite element method to investigate their behaviour at ambient and elevated temperatures due to fire. The analysis encompasses the effect of the coupling and the endplates' thickness on the cellular beams' collapse strength considering the initial geometric imperfections and material nonlinearities. A parametric study including changing temperature, cross-section geometry, and web aperture configurations was done for beams subjected to uniform bending and distributed load. The analyses depicted the following failure modes: LTB and LTB+ plastification of the two T-section (P-2 T) for end moment load and yielding of top tee section's flange (B-1 T), P-2 T, web post-buckling (WPB), Vierendeel mechanism (VM) and LTB for a distributed load. Combined failure modes such as LTB + WPB, LTB + VM and LTB + VM + WPB have also been observed. Buckling curves for cellular beams were assessed by comparing FE reduction factors with those of the buckling curve recommended by Eurocode 3 for equivalent solid steel beams. A new proposed formula for the plateau length of the LTB curves was obtained, based on the mean squared error method (MSE) between the numerical results and Eurocode formulae. The comparison between the numerical and the simplified design method predicted results shows that the proposed formulae have reduced the discrepancy and improved the LTB curve to better assess the cellular beams behaviour.

1. Introduction

Cellular steel beams bring sustainable and innovative alternative solutions for modern building construction to achieve longer spans and open spaces with additional advantages for service integration through the beam's depth. This type of beam is primarily produced by thermally cutting parent European hot-rolled sections and reassembling them in two shifted parts to fabricate beams with evenly spaced smooth round web openings.

Research studies on the behaviour of unrestrained open-web steel beams at ambient temperature or under fire have been stimulated by the demand of the construction industry for innovative cellular beams.

However, with the presence of openings as the cross-section height increases, the beams are prone to a variety of failure modes and instability at ambient temperature [1]. Several research works studied the effect of such modes with particular emphasis on web-buckling for castellated [2] and for cellular beams [3–6] which was proved to be significant at posts between closely spaced web apertures. The other instability mode, the Vierendeel mechanism, was investigated by authors [3] on cellular steel beams and an empirical shear moment interaction curve was provided.

The LTB problem in cellular steel beams, explained by the compressed tee being insufficiently supported laterally, have been reported in a significant number of experiment [4,7]. There are two distinct

---

groups of design guidelines, for LTB, the one based on the 1 T approach is considered very conservative [7,8] and the one based on the 2 T approach which has been adopted in the current proposals [9,10]. In the latter, the choice of the buckling curve is different from one proposal to another. Nseir et al. [7], Boissonnade et al. [11] and later prEN 1993–1-13 [12] recommended to use the buckling curve 'c' of the EC3 part 1–1 [13]. The studies of Panedpojaman et al. [10] for cellular beams recommended the use of the general case curves of EC3. In a recent research, Ferreira et al. [14] emphasized that possible updates on EC3 formulation would lead to LTB resistance of cellular steel beams without any correction as a function of shear stress for different load configurations. More recently, researchers have used intelligence methods, such as artificial neural networks (ANN) [15,16] and least square support vector machines LSSVM optimized by metaheuristic algorithms [17] to solve problems involving the prediction of LTB resistance of steel cellular beams.

Steel beam members require a base level of resistance against fire [18] to prevent precocious failure when unprotected and if this is not met the sections for solid or cellular beams may be protected. Baily [19] was the first to conduct a fire test on unloaded solid and cellular beam samples with a primal concern of comparing the temperature elevation and distribution between protected and unprotected sections. Mesquita et al. [20] carried out experimental and numerical research to study the critical temperature of laterally unrestrained solid steel I-beams under fire conditions. Based on the experimental study findings of Nadjai et al. [21], Vassart et al. [22] proposed an analytical calculation method to determine the WPB strength of cellular beams during fires. Ellobody et al. [23] found out that the use of castellated steel beams in composite frames led to less vertical mid-span deflection than frames without them, as well as improved span-to-maximum deflection ratios. The experimental results of Mesquita et al. [24] and Lamri et al. [25] on unloaded solid and cellular beams in fire conditions with and without intumescent fire protection indicated intumescent coating efficiency when applied to solid beams as well as cellular beams, Wang et al. [26] indicated that the degree of protection of the hole edge has a significant impact on the temperature distribution in the web post, which subsequently influences the buckling behaviour of the web post, thereafter, Nadjai et al. [27] came to confirm that the intumescent coating is the most efficient fire prevention material for the steel cellular beams.

Regarding unprotected cellular beam members, a new normative appendix, Annex F, on Beams with Large Web Openings, is included in the updated first draft of prEN 1993–1-2 [28], in which the section factors for the cellular beam's different failure modes in fire was the focal point. Nevertheless, for the LTB mechanical response under fire, no provision was made considering geometric imperfections effects, residual stresses, material, and geometric nonlinearities. Furthermore, only a few research has been done on this subject [22,29]. Recent investigations are yet to reach a full understanding of the LTB resistance and failure modes with the factors mentioned above [30–33]. Kada et al. [34] presented a numerical study on the flexure of beams with hexagonal and circular web apertures under fire conditions for several uniform load levels. Silva et al. [31] investigated the LTB behaviour of solid and cellular steel beams by relating temperature to various geometric parameters, and proving that short beams with a small tee height fall due to the Vierendeel mechanism (VM), while higher tee height fails due to web-post buckling (WPB). Correa de Faria et al. [33] caried out a FE analysis and an extensive parametric study to formulate a procedure for evaluating the LTB resistance of cellular steel beams, as well as address the issue of the elastic critical moment for cellular beams under non-uniform bending. It has been demonstrated that numerical and analytical results on the elastic critical moment vary significantly (up to 10% under uniform bending, 25% under non-uniform bending) for cellular beams with non-dimensional slenderness below 2.0 at room temperature and 3.0 in fire situations. Benyettou et al. [32] addressed numerically the LTB failure mode of beams having closely spaced large openings and the influence of parameters such as length, height of the

cross-section, opening diameter and the effect of residual imperfections on their fire resistance.

Given these points, there is a need for more research on LTB resistance of cellular steel beams and especially when failure modes and their interaction are to be considered and when the adequate LTB curve is chosen. In this paper, numerical models are developed to predict the LTB behaviour of unrestrained cellular steel beams and their effective solid beams at increasing elevated temperatures due to fire. Through these numerical models, it is sought to fill the gaps that previous works overlooked concerning the determination of the appropriate LTB elastic critical moment, the depicted interacting failure modes such as WPB; VM and yielding of the Tee section, the influence of buckling curve choice and of geometric parameters on the LTB buckling strength of such beams. The simulations carried out with the finite element software ANSYS APDL [35], included the initial geometrical imperfections, residual stresses, and geometric and material nonlinearities. To evaluate the fire resistance of a cellular beam, it was necessary to analyse and compare the obtained numerical results with the analytical design methods available in standards and literature. To do so, the LTB curve of the effective solid beam has been chosen for the calculation of LTB resistance of the cellular beam and confronted with the results got when using the LTB curve "c" recommended by [12]. Furthermore, a parametric study was conducted to identify the influence of variation of cross-section dimensions, opening geometric characteristics, steel beam length and non-dimensional slenderness on the CB's fire resistance and failure loads considering the instabilities, and consequently on the stress distribution along the beam span. The numerical predictions of the failure modes and the related load-carrying capacity were compared to the calculation methods from [12,13,18,36].

2. The influence of imperfections for solid and cellular beams

Imperfections to be considered are of two kinds geometric and residual stresses which are linked to the prescribed straightness tolerances of the beam and induced stresses and both are included in the design by EC3–1-1 [13].

The presence of imperfections in cellular beams significantly impacts their structural performance reducing the load-carrying capacity [15,37]. According to Martins et al. [38] and Rossi et al. [39], geometrical imperfections, such as initial curvature, in beams, alters the traditional buckling problem and transforms it into a load-displacement problem, which stands in opposition to the problem of bifurcation of the equilibrium. Thus, the consideration of geometric imperfections in numerical analysis is essential for obtaining accurate results, which is indispensable when predicting the behaviour of steel structures. Teixeira et al. [40] concluded in their study that geometric imperfection shape has a marked effect on the outcomes of the simulation, both qualitatively in terms of altering failure modes and quantitatively by increasing the overall resistance due to web bending. Boissonade et al. [41] suggested that using eigenmodes as the initial imperfect shape is appropriate, provided that the initial amplitude is carefully scaled (e.g. L / 1000).

Measurements of residual stresses are a major issue and research works done [42] aimed to better quantify these stresses for different types of components and subsequently include them in improved design rules and advanced numerical models. Nseir et al. [7] highlighted the complexity of the state of residual stresses in cellular beams and proposed a solution to account for their effects by adopting the amplitude L/500. The numerical study by [9] proposed a residual stress pattern for cellular I-beams and concluded that the residual stress modification affects the LTB buckling resistance. The suggestion of the use of the EC3 buckling curve c for non-dimensional slenderness for LTB $\overline{\lambda}_{LT} < 1.25$ and buckling curve b for $\overline{\lambda}_{LT} \geq 1.25$ overestimate the LTB resistance because the real distribution of residual stresses on cellular steel beams cross section lowers the buckling resistance. Abambres and Quach [43]

presented a review of available analytical approaches on residual stresses and clearly emphasized that these are often required as input for numerical analyses.

Recent numerical investigation on residual stresses conducted by Silva et al. [31] suggested new models that account for the cutting and welding phases of the plates used in the manufacture of steel cellular beams. It was concluded that with considering or not the residual stresses on the web, the beam's resistant capacity remains the same, and even their ways of collapse remain the same.

The present work adopts residual stress patterns, Fig. 1, from Silva et al. [31] and were used as incoming data in the following parts which relate to the studies of the lateral torsional buckling.

3. Design rules for the resistance of cellular beams

Research works seek to provide current codes with adequate formulations for the ultimate resistance of cellular beams, and improved analytical models have been developed to establish design rules especially for the Eurocode [10,33,36,44].

This part addresses solid and cellular beams resistance at ambient and elevated temperature for flexural, LTB for gross and net section. The net section corresponds to the 2 T cross-section at the opening's location in a cellular beam, and the gross section is the I-cross section's overall area, excluding any holes within the cross section (see Fig. 2).

The geometric dimensions of the above shown beam are overall breadth (b); flange thickness (t_f); web thickness (t_w); web opening diameter (a_0); final height (H); web depth of solid web section ($h_w = H - 2 * t_f$); web depth of one Tee-section ($h_{wT} = h_w/2 - a_0/2$); spacing between the web openings (S); web post width (S_0).

Design according to [12,13] is conducted when considering the final height H for the solid/cellular cross sections with the same class 1 or 2 as the original parent section. The 2 T approach is adopted to study cellular beams, with cross-sectional characteristics computed at web's opening center, using the Eurocode's buckling curves for the equivalent rolled I-section.

3.1. Design resistance at ambient temperature

The plastic bending design resistance ($M_{pl,Rd}$) for solid cross-section is based on the formulation available in EC3–1-1 clause 6.2.5 [13]. The flexural bending design resistance for a cellular beam cross-section is expressed as [36]:

$$M_{Pl.Rd.2T} = w_{pl.2T} f_y / \gamma_{M0} = 2 A_T Z_c f_y / \gamma_{M.0} \tag{1}$$

$$Z_c = \left(A_f \left(h_w + t_f \right) / 2 + A_{wT} (h_{wT}/2 + a_0/2) \right) / \left(A_f + A_{wT} \right) \tag{2}$$

where: $w_{pl.\ 2T}$ is the plastic section modulus of the two Tee sections; f_y is the yield strength at 20 [33]; Z_c is the distance between the local centroid of one Tee section's area and the global one; γ_{M0} is partial factor for resistance of cross-sections whatever the class is equal to 1; A_T is the area of one Tee section, $A_T = A_f + A_{wT}$; A_f is the area of the flange of one Tee; A_{wT} is the area of the web of one Tee section.
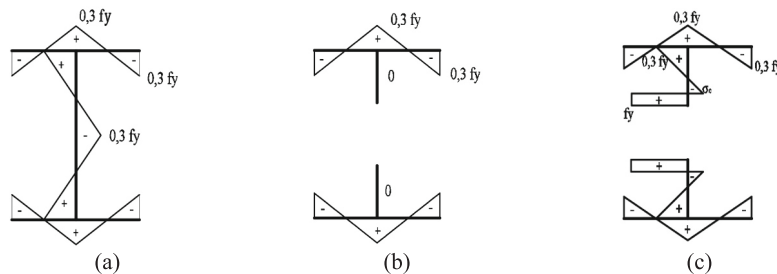
The lateral torsional buckling resistance ($M_{b.\ Rd}$) of a laterally unrestricted beam is calculated using the Eq. (3) for solid and cellular members [12,13].

$$M_{b.Rd} = \chi_{LT} w_{pl.y} \frac{f_y}{\gamma_{M1}} \tag{3}$$

where: $w_{pl.\ y}$ is the plastic section modulus of the gross and the 2 T sections respectively; γ_{M1} is a partial safety factor equal to 1; χ_{LT} is the reduction factor for lateral-torsional buckling which can be calculated according to the "general case" of EC3, and given by Eq. (4).

$$\chi_{LT} = \frac{1}{\Phi_{LT} + \sqrt{\Phi_{LT}^2 - \overline{\lambda}_{LT}^2}} \ but\ \chi_{LT} \leq 1.0 \tag{4}$$

With $\Phi_{LT} = 0.5 \left[1 + \alpha_{LT} (\overline{\lambda}_{LT} - 0.2) + \overline{\lambda}_{LT}^2 \right]$, α_{LT} the imperfection factor related the appropriate buckling curve, and $\overline{\lambda}_{LT}$ is the appropriate non-dimensional slenderness given by Eq. (5).

$$\overline{\lambda}_{LT} = \sqrt{\frac{w_{pl,y} f_y}{M_{cr}}} \tag{5}$$

M_{cr} is the elastic critical moment calculated as the maximum value of bending moment supported by a beam free from any type of imperfections [45]. M_{cr} for the net section is calculated taking into account the torsion constant (I_t), and the warping constant (I_W) according to [10].

3.2. Design resistance at elevated temperatures

The simplified rule for the design resistance in a fire situation is determined from the one of the normal situation [13] taking into consideration steel's mechanical characteristics at high temperatures [18]. The flexural design resistance of the gross and net sections ($M_{fi.\ \theta.\ Rd}$; $M_{fi.\ \theta.\ Rd.\ 2T}$), at a specific elevated temperature θ is obtained by multiplying the above mentioned resistances at 20 °C ($M_{pl.\ Rd}$; $M_{Pl.\ Rd.\ 2T}$), by the reduction factor for the yield strength of steel at temperature θ, reached at time t, $k_{y.\ \theta}$, and replacing γ_{M0}, γ_{M1} by $\gamma_{M,\ fi}$, in which $\gamma_{M,\ fi}$ is the partial factor for the relevant material property for the fire situation. The elastic critical moment $M_{cr,\ \theta}$ of the gross and net cross-sections at a specific elevated temperature θ is obtained by multiplying the above-mentioned resistance M_{cr} at 20 °C by the reduction factor for the slope of the linear elastic range at the steel temperature θ, reached at time t, $k_{E.\ \theta}$.

The lateral torsional buckling resistance, $M_{b.\ fi.\ t.\ Rd}$ of gross section and $M_{b.\ fi.\ t.\ Rd.\ 2T}$ of net section, is computed as for normal conditions considering the reduction factor in the fire situation, $\chi_{LT.\ fi}$ [18]. Similarly, $\chi_{LT.\ fi}$ is determined based on formulations at ambient, where:

$$\Phi_{LT.\theta.com} = 0.5 \left[1 + \alpha\, \overline{\lambda}_{LT.\theta.com} + (\overline{\lambda}_{LT.\theta.com})^2 \right] \tag{6}$$

$$\alpha = 0.65 \sqrt{235/f_y} \tag{7}$$

$$\overline{\lambda}_{LT.\theta.com} = \overline{\lambda}_{LT} \left[k_{y.\theta.com} / k_{E.\theta.com} \right]^{0.5} \tag{8}$$

Fig. 1. Residual stress distribution models, a) for solid beam, b-c) for cellular beam.
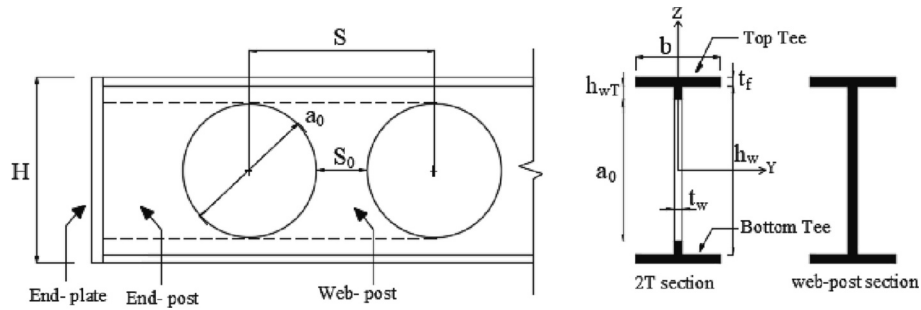
Fig. 2. Geometric properties of cellular steel beams.

$k_{E. \theta. com}$ is the reduction factor for the slope of the linear elastic range at the maximum steel temperature in the compression flange $\theta_{a. com}$ reached at time t.

New design formulations for α and $\chi_{LT. fi}$, Eqs. (9) and (10), to consider the bending moment distribution, the type of cross section, and steel grade are introduced to improve the design efficiency [46].

$$\alpha = \beta\sqrt{235/f_y} \tag{9}$$

$$\chi_{LT.fi.mod} = \frac{\chi_{LT.fi}}{f} \le 1.0 \ with \ f = 1 - 0,5(1 - k_c) \tag{10}$$

where: β is the severity factor that is equal to 0.75 for h/b > 2, for rolled I-section with steel grade S355, $\chi_{LT. fi. mod}$ is a modified reduction factor, k_c is a correction factor equals to 0.91 for parabolic moment distribution and equals to 1.0 for constant moment distribution.

4. Definition of the parametric analysis and case studies

The parametric study, of the hot-rolled profile, IPE450, with class 1 and 2 cross-sections, is the focus of the research for simply supported solid and cellular steel beams subjected to LTB following the assumptions below.

4.1. Assumptions

The following assumptions according to the EC3–1-13 [12], the SCI reference [36], and the ArcelorMittal catalogue [47] are made, regarding the properties of the beam model in the numerical simulations:

- Cellular beams with I profile, which are symmetric about the weak axis, with $h_{wT} > t_f + 30$ mm, the ratio of the depth of top and bottom Tees $0.5 \le h_{wT,b} / h_{wT,t} \le 3$, [36];
- Regular circular openings are the main configuration of openings that are used, openings placed centrally in the depth of the section $h_{wT,b} / h_{wT,t} = 1$, with web-post width; $a_0/12$ or 50 mm $< s_0 < 0.75 \ a_0$ [47],
- Large web openings in which $1.25 \ a_0 < H < 1.75 \ a_0$ [47],
- Closely spaced circular openings: edge to edge spacing $s_0 < a_0$ and the minimum end-post width s_e is $0.5 \ s_0$ [12], $s_e \ge 0.5 \ a_0$ [36],
- The LTB for cellular beams is mainly affected by residual stresses applied along the cross-section.

4.2. Geometric parameters of studied cases

Studied related cases, SB, and CB, are considered with respect to, the beam span L, the cross-section depth H, and the load type for both solid and cellular beams, and to opening diameter a_0, spacing S for the latter, see Table 1. Two different load cases were applied to the beams: end moments (M) uniform distributed (D). Geometrical parameters for

Table 1
Geometric and loading data for solid and cellular steel beam cases.

Beam	Parent steel profile	Loading type	H	a_0	S	L (m)
Solid	SB	IPE450				
			M	1.3h	–	–	2, 3, 4, 5, 6, 8, 10, 12, 14
				1.4h			
				1.5h			
			D	1.3h			3, 4, 5, 6, 8, 10, 12, 14
				1.4h			
				1.5h			
Cellular	CB	IPE450				
			M	1.3h	0.8h	1.1a_0	2, 3, 4, 5, 6, 8, 10, 12, 14
				1.4h	1.0h	1.4a_0	
				1.5h	1.2h	1.7a_0	
			D	1.3h	0.8h	1.1a_0	1.5, 2, 3, 4, 5, 6, 8, 10, 12, 14
				1.4h	1.0h	1.4a_0	3, 4, 5, 6, 8, 10, 12, 14
				1.5h	1.2h	1.7a_0	

cellular beams were varied proportionally to the parent section height, h, and to the opening diameter, a_0, see Table 1. Different opening sizes and spacing were selected to include geometries at the lowest, intermediate, and high limits of a_0/h and S/a_0 within the recommended range of assumptions.

For LT buckling analysis, designations are given for the cellular beam models according to their geometric properties. The first symbol on the label indicates the section, and the second and third symbols represent the opening ratio (a_0/h) and spacing ratio (S/a_0), respectively. Thus, for example the label CB-0.8-1.1 refers to the cellular beam of a cross-section IPE450 with $a_0/h = 0.8$ and $S/a_0 = 1.1$.

The geometry and position of the web aperture influence the in-elastic buckling load [15]. It is worth noting that the number of openings is odd for all the studied cases, so that one cell is always located at the beam's mid-span submitting the 2 T-section to the highest bending moment. Applied uniformly distributed temperatures are, room temperature $\theta = 20 °C$, and two high temperatures, $\theta = 500 °C$ and $700 °C$ chosen for a fire situation. The steel grade S355 ($f_y = 355$ (MPa)) was used for all beams with a typical value of elasticity modulus of 210 (GPa), and Poisson's ratio of 0.3.

5. Numerical model, boundary conditions, and imperfections

5.1. Finite element model description and boundary conditions

A total of 1548 FE beam models make the set of numerical simulations performed, using the ANSYS software package [35], to study the LTB resistance of laterally unrestrained beams, with and without web openings. The 3D four-node shell element type SHELL181, with full integration, was used, without considering the fillet radius between the web and the flanges. Mesh sensitivity analyses were carried out for elements sizes equal to 30 mm, 20 mm, and 15 mm, using both the elastic buckling moment and ultimate collapse moment for comparison, see Table 2. The numerical results are compared with the elastic critical moment and the LTB moment resistance given by Eurocode, as defined in Section 3. From these simulations, an element size of 20 mm, see Fig. 3, for all simulations was chosen, considering the required accuracy and acceptable computation times.

Beam end conditions, designed to create "fork" type supports, are modelled by restraining the two ends by, the vertical displacements (U_y) on the bottom flange, the lateral, out-of-plane, displacements (U_x) along the web, the rotation along Z (ROTZ) on the bottom flange and the web, Fig. 3. All nodes at mid-span are axially restrained (U_z) and the rotation (ROTX) of nodes of beam ends sections are coupled to the chosen master node at the web centre defining a rigid region (CE), where the given master node's rotation is the same for all nodes. End plates, with one time the flange thickness, are added to the beam to avoid web local crippling and section plastification. These plates should be capable of transmitting vertical shear and enabling beam end rotations without producing large moments [48]. For cases involving short and high section cellular beams, where the first buckling mode is local buckling or a mix of local and distortional buckling rather than lateral torsional buckling, Coupling (CP) degree of freedom, set for the ROTZ, was applied during the Eigen buckling analyses along the all beam span studied with distance of S/2 and H/2 for cellular and solid beams, respectively, to account for the web strengthening against local buckling thereby promoting the LTB collapse mode. Applied loads on the model are pure bending moments, M, achieved by a couple of forces in the form of uniform loading applied at the top and bottom flanges of the beam end sections or the mechanically distributed load, D, applied on the node's top flange centreline.

5.2. Mechanical model and imperfections

Both material and geometric nonlinearities are considered, as well as imperfections such as residual stresses and initial geometrical out-of-straightness. The stress-strain relationship defined by the Eurocode 3 Part 1–2 [18] is used for the simulations. Geometric imperfections are considered with an amplitude value of L / 1000 by [9,41] for solid and cellular steel beams respectively, where L is the beam span. At room and elevated temperature conditions, residual stresses for solid and cellular beams were modelled as an initial stress state condition, as presented in Fig. 4. All studies were carried out using the Newton–Raphson solution process.

5.3. Numerical model validation

The numerical model described in the previous sections was employed to the experimental tests of cellular steel beams of Sonck et al. [8,9] following the same procedure as Faria et al. [33]. Two experimental tests done with cellular beams subjected to four-point bending were simulated and the load-displacement curve were compared. Table 3 shows the specimen's geometric details, with $f_{y,f}$ and $f_{y,w}$ being the yield strengths of the flange (top and bottom flanges) and the web, respectively. E is the elastic modulus, L and L_f are, respectively, the total beam length and the distance between loads. The tests were done at room temperature.

Fig. 5 presents load versus vertical displacement from the numerical results (FE), at the loading points and mid span, in comparison with the experimental results (EXP), measured at the loadings points. For the 3.15 (m) length beam, the numerical collapse load was 23.56 (kN) and the experimental value is 22.34 (kN) [8]. In the case of the 3.99 (m) beam length, the numerical collapse load obtained was 24.50 (kN) and the experimental maximum load was 23.62 (kN). The overall load and displacement curves agree satisfactorily well with the experimental behaviour, and the numerical model failure mode was LTB as the one obtained experimentally. The difference between experimental and numerical results are 5.5% and 3.7% for the CS2_L3 and CS2_L4 specimens, respectively. Considering the simplified residual stress pattern used in the model and its influence in the failure load [8,9] and as the real geometric imperfections were not modelled but a global imperfection, with maximum amplitude of L/1000, the numerical results are acceptable, and the model considered suitable for further analysis.

6. Simulations for LTB elastic critical moment, and effect of coupling and end plates

Analytical and numerical simulation results are presented for the LTB resistance of cellular beams, with two thorough investigations. The first is for the LTB elastic critical moment at ambient and elevated temperature, and the second is for the effect of coupling, as well as the end plates' thickness on the collapse resistance at ambient.

6.1. LTB elastic critical moment

The LTB elastic critical moments, under ambient and elevated temperatures for solid (SB) and cellular beams (CB) subjected to end moment or distributed loads, are determined by linear buckling analyses carried out using the FE software ANSYS [35]. The FE critical LTB moments (M_{cr},FE) were compared with analytical critical moments ($M_{cr},EC3$) using the I and 2 T approach for solid and cellular beams, respectively. The differences in this comparison as a percent error versus the numerical non-dimensional slenderness are plotted in Fig. 6. The numerical non-dimensional slenderness to LTB at normal $\bar{\lambda}_{LT,FE}$ and at elevated temperature $\bar{\lambda}_{LT,\theta,FE}$ were determined by following the same approach of the analytical method, Eqs. (5) and (8) in Section 3, but considering the corresponding plastic moment resistances and elastic critical moments. The FE in-plane bending resistance was calculated using the numerical beam models that have been subjected to end moment loads.

From the extensive simulations performed at room temperature and in a fire situation, the global LTB mode was identified as the first buckling mode, for both loading types, for over 80% of cases.

Fig. 6 (a) shows that for end moment loading case, and at target temperatures of 20, 500, and 700 °C, the percentage differences between the two sets of results vary from −1.99% to 1.04% for the case of SB, and from −6.1% to 6.5% for the case of CB. Fig. 6 (b) shows that for the distributed loading case, the differences were <2.5% for SB cases, and were divided into two groups depending on whether the $\bar{\lambda}_{LT}$ is greater or <1.5 for CB cases. For $0.5 \leq \bar{\lambda}_{LT} \leq 1.5$ corresponding to a span of 3 m,

Table 2
Mesh sensitivity analysis, cases with H/h = 1.3 h, a0/h = 0.8, S/a0 = 1.1, L = 5. m.

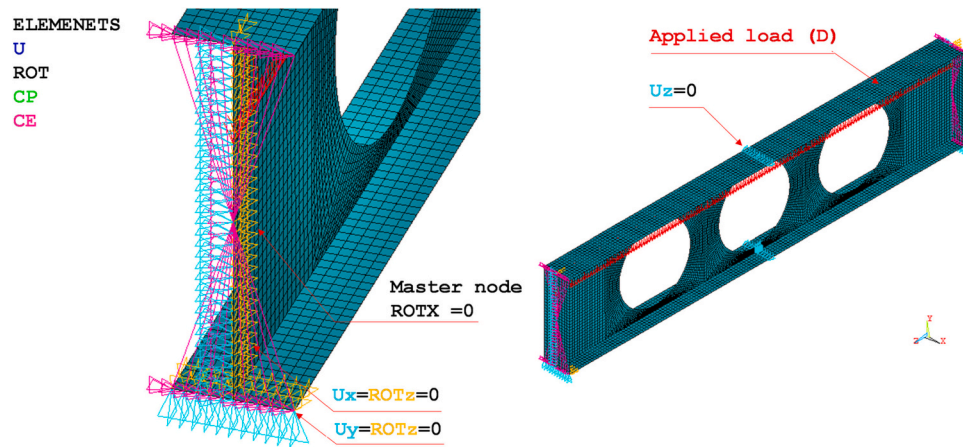| Analysis type	M_{EC3} (kN. m)	Element size	M_{FE} (kN. m)	M_{FE} / M_{EC3}
Elastic buckling analysis	453.855	15 mm	457.103	1.007
		20 mm	458.043	1.009
		30 mm	460.116	1.014
Nonlinear analysis (NLGMA)	320.635	15 mm	355.288	1.108
		20 mm	355.599	1.109
		30 mm	356.785	1.113

Fig. 3. Mesh configuration of FEM and boundary conditions for IPE base profile cellular steel beams (L = 3 m, H/h = 1.4, a_0/h = 1.2, and S/a_0 = 1.4).
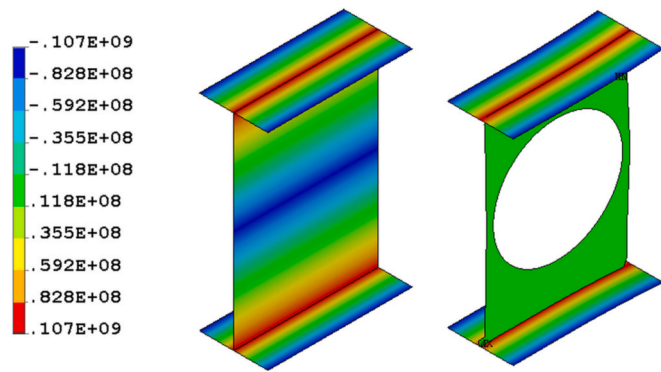

Fig. 4. Residual stress distributions of rolled sections, S355: (a) solid beam; H = 1.3 h, (b) cellular beam; H = 1.3 h, a_0 = 0.8 h.

the LTB buckling mode was observed to be associated with web distortion, which has induced a larger discrepancy between numerical and analytical elastic critical moments. Discrepancies for 5.6% of cases vary from −10% to −35%. For $\bar{\lambda}_{LT} \geq 1.5$ corresponding to spans of 4 m and over, the lowest and largest relative errors were 0.03% and 9%, respectively. As beam length increases the effect of web distortion decreases.

The analytical and the FE results were in excellent agreement, and owing to the small discrepancies, the numerical model was considered validated for computations of LTB elastic critical moment M_{cr}.

6.2. Effects of coupling and end plates' thickness on the collapse resistance of cellular beams

The coupling procedure, CP, was used in all the studied solid and cellular beam models' Eigen buckling analyses, as is alluded to in Section 5. In this part, the effects of the end plates and the coupling on the LTB

Table 3
Geometric details of test specimens.

Specimen	H	b	t_w	t_f	a_0	S_0	n	L	L_f	$f_{yt,f}$	$f_{yb,f}$	$f_{y,w}$	E
	(mm)	(mm)	(mm)	(mm)	(mm)	(mm)		(mm)	(mm)	(MPA)	(MPA)	(MPA)	(MPa)
CS2_L3	220	83.1	5.5	7.3	142.8	67.2	15	3150	210	342	341	329	205
CS2_L4	220	83.1	5.5	7.3	142.8	67.2	19	3990	1890	348	351	339	205
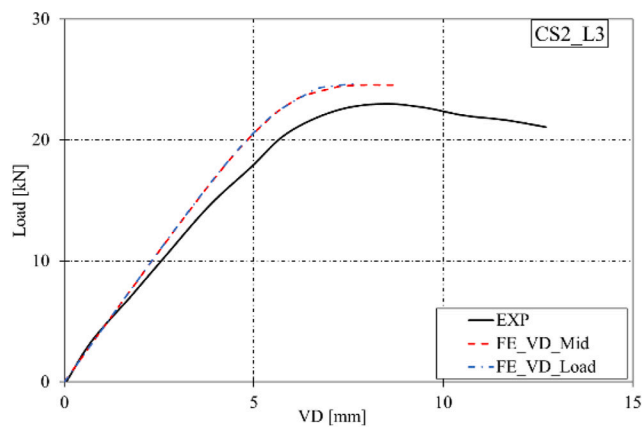
(a) Case CS2_L3
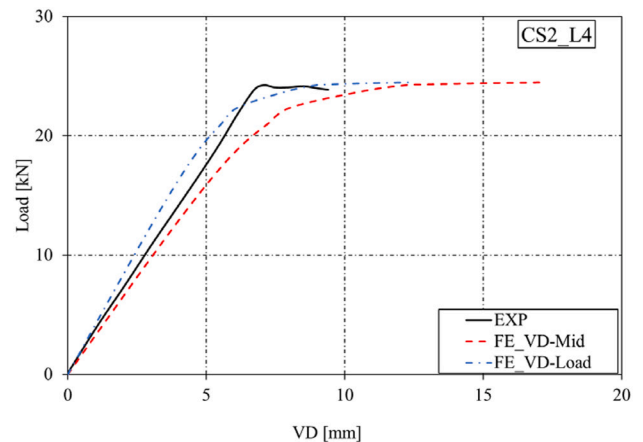
(b) Case CS2_L4

Fig. 5. Comparison between numerical and experimental tests. Load versus vertical displacement.

(a) End moment loading M

(b) Uniformly distributed load D

Fig. 6. Analytical and numerical LTB elastic critical moments percental differences for solid and cellular beams at θ = 20 °C and θ = 500, 700 °C.
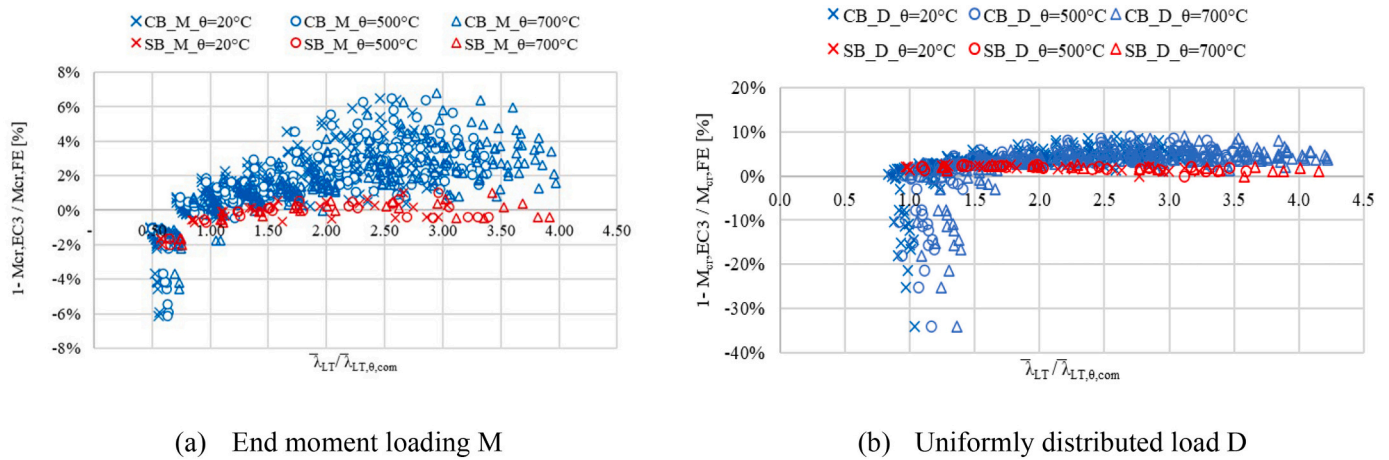
capacity and the related failure mode at ambient temperature is demonstrated for the non-linear FE model.

Four models are considered, each with a specific configuration was analysed for various conditions: Model 1: refers to the model without endplates (W/O.EP) and without coupling (W/O.CP), Model 2: without endplates (W/O.EP) and with coupling (W/CP), Model 3: with endplates of 2*tf thickness (W/EP.2*tf) and with coupling (W/CP) and Model 4: with endplates of 1*tf thickness (W/EP.1tf) and without coupling (W/O. CP). Table 4 lists all the analyses done, and corresponding results, where the collapse moment M_{COLL} is compared with the EC3 results [13], $M_{b,Rd,2T}$. The investigated cellular beams of various span lengths, which subjected to uniformly distributed load, had a beam height to parent section height ratio of 1.3, an a_0/h ratio of 0.8, and an S/a_0 ratio of 1.1.

A comparison of the results of models 1 and 4 showed that the presence of EP resulted in an average 5.2% increase in collapse load resistance when compared to EC3 calculations. In the absence of end plates, results indicated deformation at the beam ends (plastic yielding PY) for spans of 5 m and less. After a comparison of Models 1 and 2, it was observed that the incorporation of numerical coupling in a nonlinear analysis impacts the performance of web posts. Interestingly, it was seen that the uncoupled Model 1 experienced failure due to WPB, whereas the coupled Model 2 resulted in plastification of the web post. Analysing model 3 for long-span beams where LTB is prevailed, a thickness of 2*t_f of EP has resulted in adverse effect on the moment resistance, with an increased gap of 42% between EC3 and FE results. Nevertheless, the adoption of a thickness of 1*t_f has resulted in

improved moment resistance of 10% -19% between EC3 and FE results.

Finally, the four models analysed revealed that numerical CP had a significant effect on the web's behaviour, regardless of whether there were plates at the ends of the beam or not. In this study, the FE model employed for the nonlinear analysis included end plates with a thickness of 1*t_f, and nodes along the beam span were not coupled. This is with the aim to implicitly trigger instability at the web post, and hence, letting the expected failure mode WPB happen.

7. Analysis for global LT buckling and interacting failure modes

The analysis for global LTB and interacting failure modes deal with a parametric study for the studied models, including the design curves, changing temperature, loading type, cross-section ratio H/h, opening ratio a_0/h, spacing ratio S/a_0, and beam span as listed in the above, Section 4. Values for H/h of 1.3, 1.4, 1.5 making three different cellular beam cross-sections, which analysed at ambient and elevated temperatures, and results for numerical resistance curves plotted with red, blue, and green colour, respectively. The analytical results are presented by dashed and continuous lines and the numerical results are plotted as single points with marks.

7.1. Buckling curves and normalized moment resistance

For uniform steel members in bending, the Eurocode 3 part 1–1 [13] identified two approaches to determine the ultimate LTB strength; the

Table 4
Effect of coupling, thickness, and existence of end plates, on the CB's collapse mode.

	L (m)	3	4	5	6	8	10	12	14
Model 1	Mb,Rd,2 T, EC3 (kN.m)	463.79	345.43	260.83	204.96	141.21	107.8	87.74	74.44
	M_{COLL} W/O.EP W/O.CP (kN.m)	250.63	224.87	244.26	211.33	150.8	123.37	97.96	84.36
	Diff (1) (%)	−85.10%	−53.60%	−6.80%	3.00%	6.40%	12.60%	10.40%	11.80%
	Collapse mode	WPB+ PY	WPB+ PY	WPB+	LTB + WPB	LTB	LTB	LTB	LTB
Model 2	M_{COLL} W/O.EP W/CP (kN.m)	338.52	255.04	276.76	227.41	157.59	121.58	97.2	90.63
	Diff (1) (%)	−37.00%	−35.44%	5.76%	9.87%	10.40%	11.34%	9.73%	17.86%
	Collapse mode	WPF+ PY	P-2 T + WPF	P-2 T + WPF	LTB+	LTB	LTB	LTB	LTB
Model 3	M_{COLL} W/EP,2t_f W/CP (kN.m)	380.69	254.84	288.81	317.44	258.06	189.13	147.16	120.9
	Diff (1) (%)	−21.80%	−35.50%	9.70%	35.40%	45.30%	43.00%	40.40%	38.40%
	Collapse mode	WPF	P-2 T + WPF	P-2 T + WPF	P-2 T + WPF	LTB+	LTB	LTB	LTB
Model 4	M_{COLL} W/EP,1t_f W/O.CP (kN.m)	272.74	236.97	258.39	222.6	158.15	123.92	102.16	92.27
	Diff [1] (%)	−70.00%	−45.80%	−0.90%	7.90%	10.70%	13.00%	14.10%	19.30%
	Collapse mode	WPB	P-2 T + WPB	P-2 T + WPB	LTB+	LTB	LTB	LTB	LTB

$$\text{Diffy}^{(1)}(\%) = \frac{M_{Coll.FE} - M_{b,Rd,2T,EC3}}{M_{Coll.FE}} * 100$$

"general case" in clause 6.3.2.2 and the "specific case" for rolled sections in clause 6.3.2.3. Depending on the cross-section, both methods are based on the concept of buckling curves and the appropriate member slenderness, but the curves to be used vary depending on whether the case is general or specific. In addition, the plateau length for the maximum non-dimensional slenderness $\bar{\lambda}_{LT,0}$ is limited to 0.2 for the general case, and 0.4 for the specific case. For slenderness values of 0.2 or 0.4, the reduction factor χ_{LT} is equal to 1. Supplementary provisions from Eurocode part 1–13 [12] extend the application of EN 1993-1-1 and EN 1993-1-5 to the design of cellular beams made from rolled and welded steel sections and recommends the buckling curve c.

The assumptions made above in Section 4.1 aimed to derive the adequate LTB curve, and the Eurocode recommendation of using buckling curve c for cellular beams requires further investigations to include a large spectrum of beam slenderness. Hence, there is also a need to clarify the lower limit of slenderness against LTB at normal temperature and therefore improve the buckling curve's tendency towards the safe or conservative state.

This study comprises analytical and numerical analyses for solid and cellular steel beams at ambient and elevated temperatures including, the in-plan plastic moment resistances, $M_{pl,Rd}$, $M_{pl,Rd,2T}$, $M_{pl,fi,\theta,Rd}$, $M_{pl,fi,\theta,Rd,2T}$, and the LTB moment resistances, $M_{b.Rd}$, $M_{b.Rd,2T}$, $M_{b.fi.t.Rd}$, $M_{b.fi.t.Rd.2T}$. Numerical analysis is carried out for different cellular beams, where collapse moment resistance M, failure modes, and stress distributions in the deformed state at the collapse time/load represent the produced results. Collapse and plastic moment resistances are used to compare analytical and numerical results. Depicted failure modes and stress distributions lead to establishing the limits of the geometric parameters such as a_0, s, and L that do not favour the predominance of the LTB behaviour.

Results are plotted for normalized FE collapse moment resistance over the in-plane bending moment resistance, $M/M_{pl,Rd}$ or $M/M_{pl,Rd,2T}$, $M/M_{pl,fi,\theta,Rd}$ or $M/M_{pl,fi,\theta,Rd,2T}$, for solid or cellular steel beams, against non-dimensional slenderness, and comparison is made with analytical curves. At ambient temperature, the flexural buckling curve b [13] is adopted for solid beams, the buckling curve b for equivalent I-sections, and the buckling curve c for cellular beams [12,13]. At elevated temperatures, the LTB resistance curves provided by ENV 1993-1-2 [18] and by Vila Real [46] are considered in addition to solid beams for cellular beams due to the lack of a dedicated explicit curve. The FE reduction factor for LTB of cellular beams is deduced from normalized collapse moment resistances, which are obtained out of the regression of the numerical resistance curves.

7.2. LTB behaviour and failure modes at ambient temperature

The numerical normalized moment resistances and analytical buckling curves for LTB are compared in Fig. 7 for each investigated beam geometry exposed to either an end bending moment M, Fig. 7 (a), or a uniformly distributed load D, Fig. 7 (b).

For applied uniform end moment, the LTB failure mode was revealed in most of the simulated cases with short and lengthy span solid and cellular beams, Fig. 7 (a). Results for FE reduction factors fit closely with the LTB buckling curve b either for the solid or cellular beams.

For CBs, with the same cross-section height, where $0, 55 < \bar{\lambda}_{LT} \leq 3.0$, the design LTB resistance was conservative by about 11% on average compared with FE resistance. However, for non-dimensional slenderness, $\bar{\lambda}_{LT} \leq 0.55$, small discrepancy between FE and design LTB resistance can be observed. This is because the LTB in combination with the 2 T-section failure (LTB + P-2 T) was identified as the dominant failure mode.

For applied uniformly distributed load, the LTB failure mode was revealed in all simulated solid beam cases, with the design LTB resistance being conservative by about 9% on average compared with FE resistance, Fig. 7 (b). On the contrary for cellular beams, failure modes occur depending on the type of geometry parameters. The collapse analysis identified the following failure modes: LTB failure; 2 T-section failure (P-2 T); yielding/bending of the top tee section's flange B-1 T, web or web post-buckling (WB or WPB); and Vierendeel mechanism VM. These failure modes are classified as either collapse by plastic yielding (B-1 T, P-2 T, VM) or collapse by instability (WB/ WPB, LTB). These results are reported in Table 5 and the non-linear analysis behaviour at the ultimate converged step is represented in Fig. 8. Additionally, the mid-span vertical displacement curves are plotted in Fig. 9, in function of the maximum applied moment normalized to the 2 T plastic moment.

LTB mode was particularly common in beam models with moderate and large non-dimensional slenderness, where the top flange's upper edge receives the most compressive stress, Fig. 8 (a). It depends on S/a_0 ratios, whatever values for H/h and a_0/h parameters. Exception is made for $S/a_0 = 1.7$, $a_0/h = 1.2$, when $H/h = 1.3, 1.4$, for beams in the interval $1.07 \leq \bar{\lambda}_{LT} \leq 1.35$, the collapse was due to VM, causing reduced resistance moment in comparison to the design curve b. For models with moderate slenderness where the LTB was the main cause of failure, there were also signs of other failure modes labelled LTB+, see Table 5, appearing in the form of stresses that were distributed around the hole or in the web post's centre, see Fig. 8 (b). The parameter ratio S/a_0, which
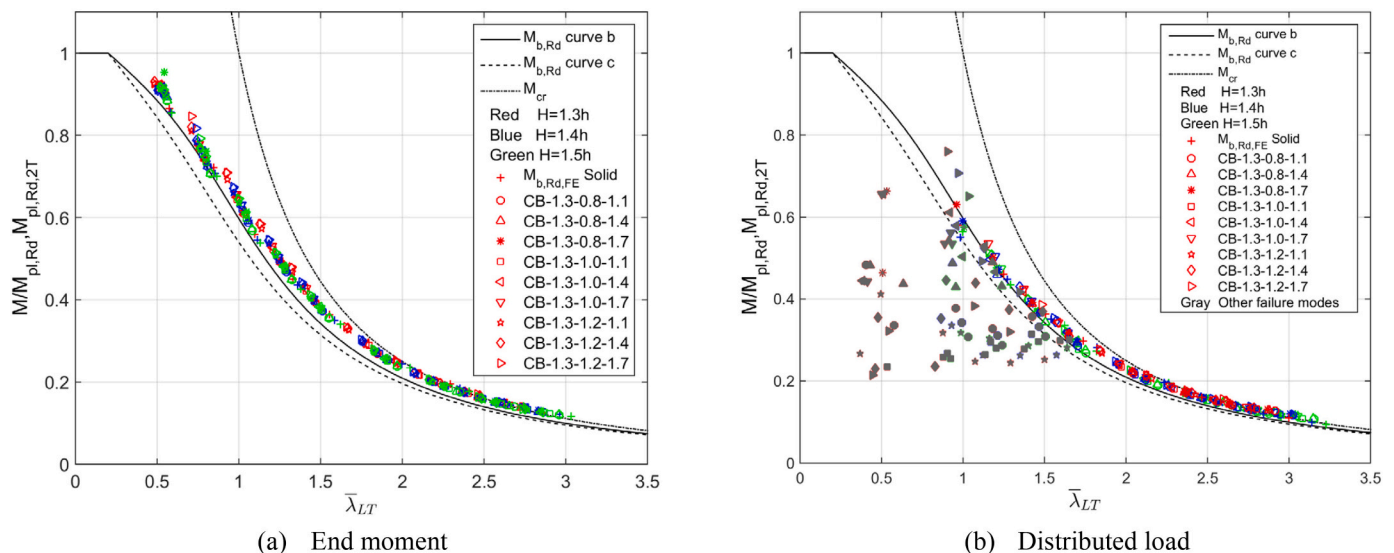

(a) End moment   (b) Distributed load

Fig. 7. Comparison between numerical normalized collapse moments and LTB analytical reduction factors versus non-dimensional slenderness at $\theta = 20$ °C.

Table 5
Summary of the failure modes related to the investigated cases at ambient temperature.

Case 1 (θ = 20 °C)	L (m)	$\bar{\lambda}_{LT,FE}$	Failure mode	Case 2	L (m)	$\bar{\lambda}_{LT,FE}$	Failure mode	Case 3	L (m)	$\bar{\lambda}_{LT,FE}$	Failure mode
CB-1.3-0.8-1.1	1.5	0.41	V + WB	CB-1.4-0.8-1.1	3–5	0.99–1.74	WPB	CB-1.5-0.8-1.1	3–5	1.03–1.51	WPB
	2–5	0.58–0.1.42	WPB		6	1.70	LTB+		6	1.75	LTB+
	6	1.65	LTB+		8–14	2.12–3.02	LTB		8–14	2.20–3.16	LTB
	8–14	2.04–2.91	LTB								
CB-1.3-0.8-1.4	1.5	0.43	V + WB	CB-1.4-0.8-1.4	3	0.94	WPB	CB-1.5-0.8-1.4	3	0.95	WPB
	2,3	0.63, 0.91	WPB		4	1.21	WPB + LTB		4	1.24	WPB + LTB
	4	1.18	WPB + LTB		5–14	1.47–3.02	LTB		5–14	1.51–3.15	LTB
	6–14	1.42–2.88	LTB								
CB-1.3-0.8-1.7	1.5	0.51	V + WB	CB-1.4-0.8-1.7	3	1.00	LTB+	CB-1.5-0.8-1.7	3	1.01	WPB
	2	0.53	WB		4–14	1.22–3.01	LTB		4	1.21	LTB+
	3–4	0.96–1.19	LTB+						5–14	1.46–3.04	LTB
	5–14	1.43–2.87	LTB								
CB-1.3-1.0-1.1	1.5	0.39	V + WB	CB-1.4-1.0-1.1	3–5	0.90–1.42	WPB	CB-1.5-1.0-1.1	3–5	0.93–1.47	WPB
	2, 3, 4, 5, 6	0.54–1.59	WPB		6	1.65	WPB+		6	1.71	WPB + LTB
	8–14	1.97–2.80	LTB		8–14	2.06–2.95	LTB		8–14	2.13–3.08	LTB
CB-1.3–1.0-1.4	1.5, 2	0.38, 0.51	V + WB	CB-1.4-1.0-1.4	3	0.96	WPB	CB-1.5-1.0-1.4	3	1.00	WPB
	3–4	0.92–1.13	VM + WPB		4	1.17	LTB + WPB + VM		4	1.20	LTB + WPB + VM
	5	1.37	VM + LTB		5–14	1.42–2.92	LTB		5–14	1.45–3.05	LTB
	6–14	1.58–2.77	LTB								
CB-1.3–1.0-1.7	1.5, 2	0.41, 0.50	V + WB	CB-1.4-1.0-1.7	3	0.92	WPB	CB-1.5-1.0-1.7	3	0.93	WPB
	3	0.89	VM		4	1.20	LTB + VM		4	1.24	LTB+
	4	1.15	LTB + VM		5–14	1.42–2.91	LTB		5–14	1.46–3.05	LTB
	5	1.37	LTB+								
	6–14	1.58–2.77	LTB								
CB-1.3–1.2-1.1	1.5, 2	0.37, 0.49	B-1 T	CB-1.4-1.2-1.1	3–4	0.93–1.12	WPB	CB-1.5-1.2-1.1	3–6	0.99–1.64	WPB
	3	0.88	VM		5–6	1.35–1.57	WPB + P-2 T		8–14	2.04–2.96	LTB
	4, 5, 6	1.07–1.50	WPB		8–14	1.95–2.81	LTB				
	8–14	1.85–2.64	LTB								
CB-1.3–1.2-1.4	1.5, 2	0.46, 0.48	B-1 T	CB-1.4-1.2-1.4	3	0.87	VM	CB-1.5-1.2-1.4	3	0.90	VM + WPB
	3, 4, 5, 6	0.83–1.49	VM		4	1.13	VM+		4–5	1.18–1.40	LTB + WPB + VM
	8	1.84–2.61	LTB		5	1.35	VM + LTB		6–14	1.63–2.94	LTB
					6	1.57	LTB+				
					8–14	1.95–2.79	LTB				
CB-1.3–1.2-1.7	1.5, 2	0.44, 0.54	B-1 T	CB-1.4-1.2-1.7	3	0.97	LTB + WPB	CB-1.5-1.2-1.7	3	1.04	LTB + WB
	3	0.91	LTB + WPB		4–5	1.12–1.35	VM		4–5	1.16–1.40	LTB + WPB + VM
	4, 5	1.07, 1.29	VM		6–14	1.56–2.76	LTB		6–14	1.62–2.92	LTB
	6	1.48	VM+ LTB								
	8–14	1.83–2.59	LTB								

represents the width of the web post, had a significant effect on the beam's collapse strength. Large values of S/a$_0$ were found to increase the maximum collapse resistance and allow the local and/or interacted failure modes to fully develop into the LTB failure mode.

WPB was detected for short spans with narrow web posts of S/a$_0$ = 1.1, see Table 5 and was also presented for cases with ratios of S/a$_0$ = 1.4 and 1.7. Fig. 8 (c) shows that for S/a$_0$ = 1.1, all web posts have reached a maximum von Mises stress distribution and only part of the web of the 2 T section near the supports. Whereas, for S/a$_0$ = 1.4 and 1.7, Fig. 8 (d), only the web posts closest to the supports were at maximum yield stress and all the web of the 2 T section of the opening at the centre line.

As mentioned on Table 5, WPB + P-2 T was related to cases with H/h = 1.4, a$_0$/h = 1.2, and S/a$_0$ = 1.1, see Fig. 8 (e).

For relatively short-length beams with H/h = 1.3, 1.4, VM was found to be dominant with relatively large tee depths a$_0$/h = 1.2, and S/a$_0$ = 1.1, 1.4, and 1.7, see Fig. 8 (f).

Interaction mode VM+ LTB has been revealed in cases with H/h = 1.3, 1.4, a$_0$/h = 1.0, 1.2, and S/a$_0$ = 1.4, 1.7, see Fig. 8 (g). The VM mode was bound to take place when the cross-section height decreased, and when H/h increases, the mode changed to VM + LTB or LTB.

VM+ WPB was observed for short beam models with H/h = 1.3, a$_0$/h = 1.0, and S/a$_0$ = 1.4 or H/h = 1.5, a$_0$/h = 1.2, and S/a$_0$ = 1.4, see Fig. 8 (h). This confirms the finding of the work by Panedpojaman et al. [5], showing that the Vierendeel mechanism may interact with buckling failure.

LTB + WPB was observed for a 4 m beam span with H/h = 1.3, 1.4, 1.5, a$_0$/h = 0.8, and S/a$_0$ = 1.4, see Fig. 8 (i). Also observed for H/h = 1.5, a$_0$/h = 1.0 and S = 1.1a$_0$, for beam span of 6 m.

LTB + WPB + VM was observed for H/h = 1.3, 1.4, 1.5, a$_0$/h = 1.0, and S/a$_0$ = 1.4, and for H/h = 1.5, a$_0$/h = 1.2, and S/a$_0$ = 1.4, 1.7, see Table 5 and Fig. 8 (j).

For cellular beams of a single opening with slenderness <0.83, short spans of 1.5 and 2 m with H/h = 1.3 were studied considering the previous parameters a$_0$/h and S/a$_0$, and the obtained results are red marked points scattered within the margin $0.37 \leq \bar{\lambda}_{LT} \leq 0.63$, Fig. 7 (b), and Table 5. For $\bar{\lambda}_{LT} \leq 0.55$, S/a$_0$ = 1.1, 1.4, 1.7, interaction between shear (V) and web buckling (WB) took place for a$_0$/h = 0.8, 1.0, Fig. 8 (k), and bending of the top tee section, B-1 T for a$_0$/h = 1.2, Fig. 8 (l).

Fig. 8 (i) shows that when shear strength is much higher, failure occurs in compression near the supports before web buckling. Fig. 8 (j) shows that von Mises stresses were higher at the flanges of the top tee section rather than at the web which is due to the transfer of axial forces and bending moments through the opening.

Fig. 10 (a) shows the change in the numerical collapse moment resistance M$_{collapse}$ with beams' length subjected to a uniformly distributed load, for web hole sizes a$_0$/h = 1.2, S/a$_0$ = 1.4, and H/h = 1.3 h, 1.4, 1.5. Fig. 10 (b) shows Von Mises stress distribution at failure for H/h = 1.3 with L = 3, 5, 8 m, labelled A, B, C, respectively, and H/h = 1.5 with L = 3, 5, 8 m, labelled D, E, F, respectively. The different changes in the M$_{collapse}$ are slenderness related that are, points A and D, B and E, C
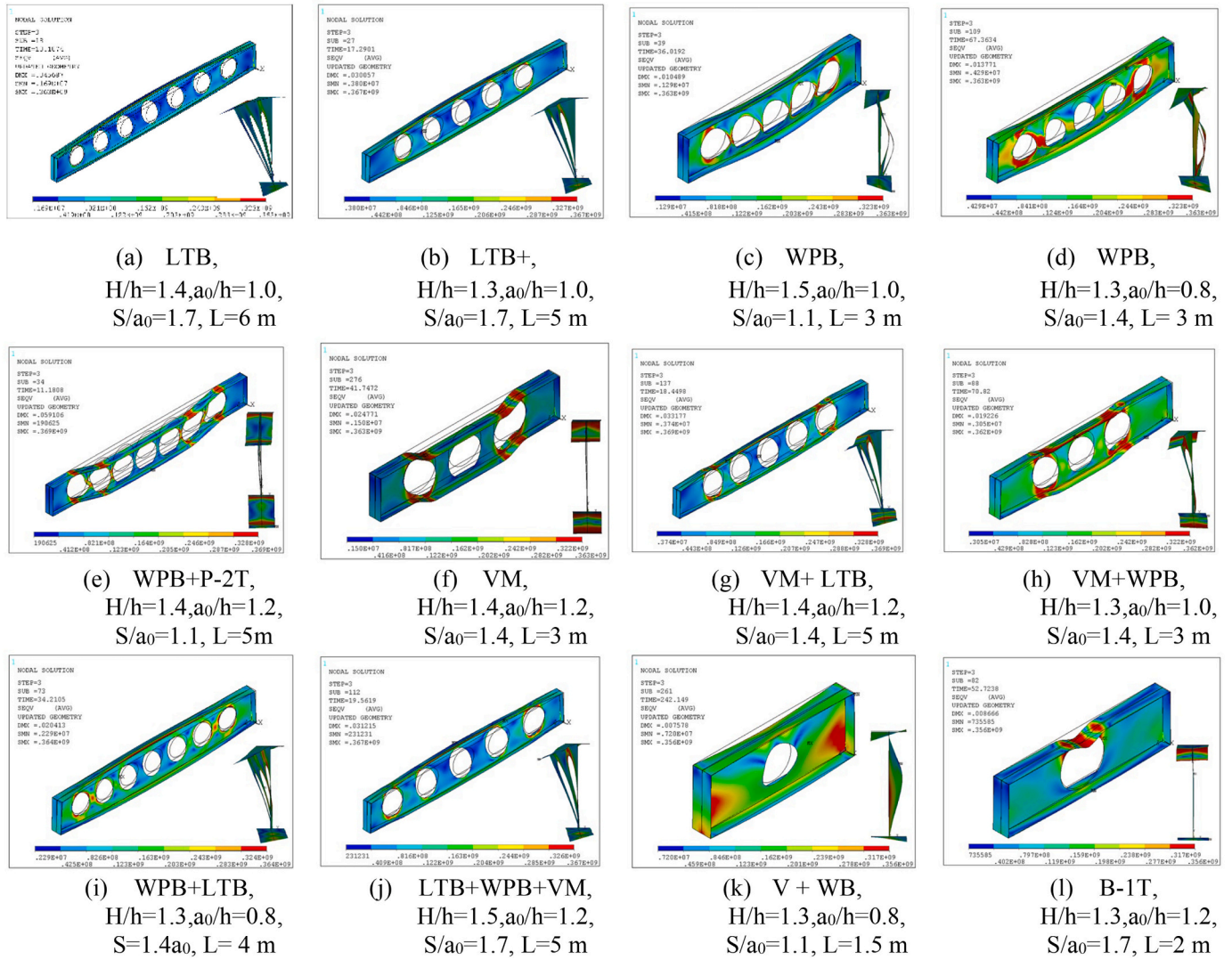
(a) LTB,
H/h=1.4,a₀/h=1.0,
S/a₀=1.7, L=6 m

(b) LTB+,
H/h=1.3,a₀/h=1.0,
S/a₀=1.7, L=5 m

(c) WPB,
H/h=1.5,a₀/h=1.0,
S/a₀=1.1, L= 3 m

(d) WPB,
H/h=1.3,a₀/h=0.8,
S/a₀=1.4, L= 3 m

(e) WPB+P-2T,
H/h=1.4,a₀/h=1.2,
S/a₀=1.1, L=5m

(f) VM,
H/h=1.4,a₀/h=1.2,
S/a₀=1.4, L=3 m

(g) VM+ LTB,
H/h=1.4,a₀/h=1.2,
S/a₀=1.4, L=5 m

(h) VM+WPB,
H/h=1.3,a₀/h=1.0,
S/a₀=1.4, L=3 m

(i) WPB+LTB,
H/h=1.3,a₀/h=0.8,
S=1.4a₀, L= 4 m

(j) LTB+WPB+VM,
H/h=1.5,a₀/h=1.2,
S/a₀=1.7, L=5 m

(k) V + WB,
H/h=1.3,a₀/h=0.8,
S/a₀=1.1, L=1.5 m

(l) B-1T,
H/h=1.3,a₀/h=1.2,
S/a₀=1.7, L=2 m

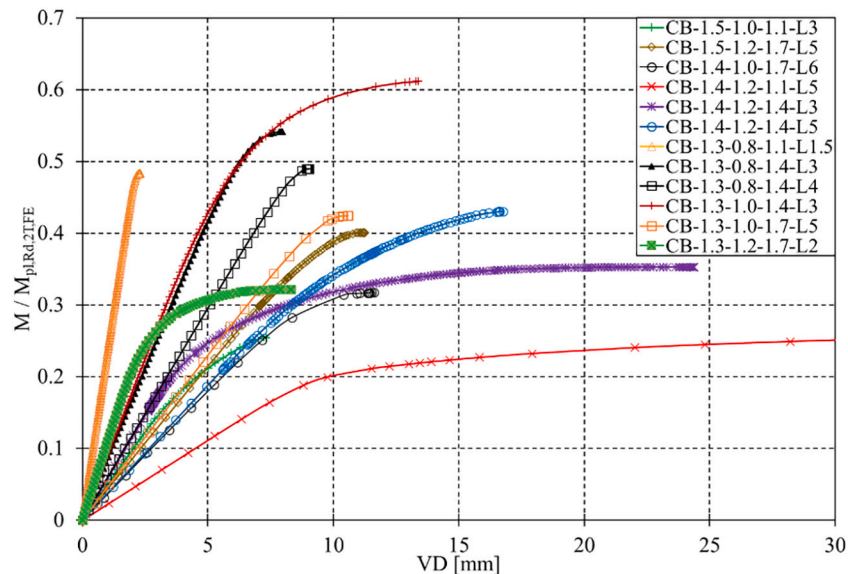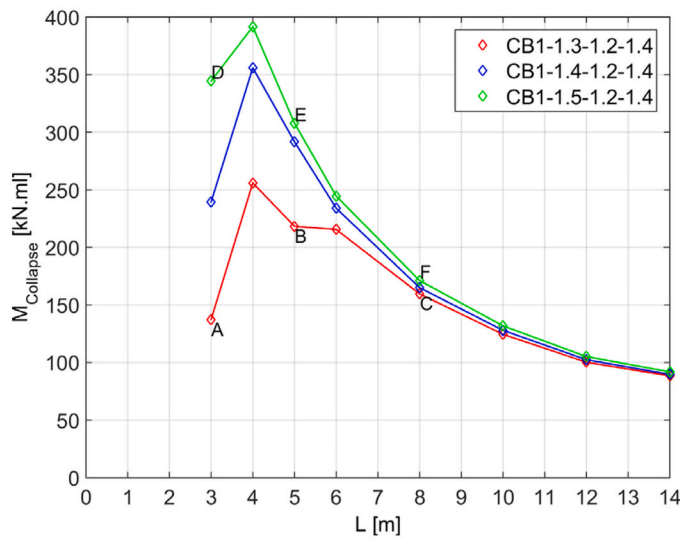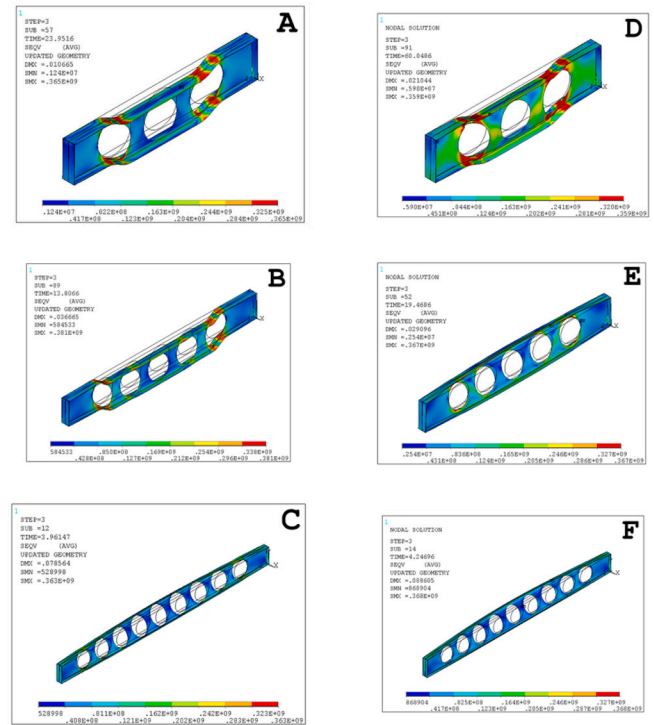**Fig. 8.** Finite element results, cellular beam deformation and collapse mechanism at failure load.

Fig. 9. Finite element results normalized applied moment versus vertical displacement at mid-span.

Fig. 10. (a) Collapse moment resistance against cellular beam lengths at $\theta = 20$ °C with H/h = 1.3, 1.4, and 1.5; $a_0/h = 1.2$; $S/a_0 = 1.4$. (b) Corresponding Von misses stress at failure for cellular beams with L of 3, 5, and 8 m.

and F for low, intermediate, and high slenderness, respectively.

It was observed that beams with low or intermediate $\overline{\lambda}_{LT}$ had experienced VM for A and B, LTB for C and F, or VM + WPB for D. The LTB failure mode occurred at high $\overline{\lambda}_{LT}$, and the higher the ratio H/h, the higher the collapse moment resistance, Fig. 10 (b). Point B, which corresponded to VM, had a significantly lower collapse moment than point E (LTB+), resulting in a reduced beam's ultimate load, Fig. 10 (a).

The final observations are:

- For higher values of S/a_0, the reduction factor χ values approach the LTB curve, and for lower values of a_0/h ratio, the LTB resistance increases.
- The cases with a WPB failure mode give, on average, a 59% difference between the numeric and analytic normalized resistances (M/$M_{pl, Rd}$, $M_{pl, Rd, 2T}$) for short cellular beams. This variation decreases to 25% for the cases of VM failure modes.
- Independently of the a_0/h ratio, it was noted that for $S/a_0 = 1.1$, 50% of all cases were on the safe side, for $S/a_0 = 1.4$, 69% of all cases appeared to be safe, and with $S/a_0 = 1.7$, >81% of all cases were safe.

7.3. LTB behaviour and failure modes under fire condition

Fig. 11 presents numerical and analytical results for solid and cellular steel beams against the non-dimensional slenderness $\overline{\lambda}_{LT,\theta,com}$ for both load conditions, end moment Fig. 11 (a, c) and distributed load Fig. 11 (b, d), for uniformly elevated temperatures 500 and 700 °C.

For applied end moment loading, the Eurocode LTB resistance curves can satisfactorily represent all FE results, as shown in Fig. 11 (a, c), at 500 °C and 700 °C, and this is also the case for solid beams subjected to distributed load.

For cellular beams with uniformly distributed loading, numerical resistance curves showed different behaviour for small and intermediate values of slenderness for temperatures, 500 °C and 700 °C (see Fig. 11

(b, d)). Table 6, and Table 7 shows the typical range of slenderness associated with each failure mechanism for each beam subjected to temperatures of 500 °C and 700 °C, respectively.

Similarly, to the analysis at $\theta = 20$ °C, the LTB failure mode was observed for intermediate and long-span beams as a function of S/a_0; with the range of $\overline{\lambda}_{LT,\theta,com}$ being dependent on the applied temperature.

WPB occurred for closely spaced openings with a ratio of $S/a_0 = 1.1$ for H/h = 1.3, 1.4, 1.5, and $a_0/h = 0.8, 1.0, 1.2$. It also occurred for $S/a_0 = 1.4, 1.7$, with $a_0/h = 0.8, 1.0$, see Table 6 and Table 7.

VM was detected for opening diameter ratio of $a_0/h = 1.2$. It occurred at 500 °C, for H/h = 1.3, 1.4 and it also occurred at 700 °C, for H/h = 1.3.

The combined failure mode LTB + WPB was observed for H/h = 1.3, 1.4, 1.5, $a_0/h = 0.8, 1.0, 1.2$, and $S/a_0 = 1.1, 1.4, 1.7$, at 500 °C and 700 °C. Combined mode, LTB + VM, was observed for $a_0/h = 1.2$, at 500 °C for H/h = 1.3, 1.4 with $S/a_0 = 1.4, 1.7$, respectively, and at 700 °C for H/h = 1.3 with $S/a_0 = 1.4, 1.7$. The last combined failure modes observed were, LTB+, LTB + WPB + VM and WPB + VM, at both temperatures 500 °C and 700 °C, see Tables 6 and 7.

Fig. 12 (a) depicts the change in the numerical collapse moment resistance $M_{fi, \theta, collapse}$ with the variation of height ratio H/h = 1.3, 1.4, 1.5, at 500 °C, by setting the ratios a_0/h and S/a_0 to values of 1.2 and 1.4, respectively. It was observed that a sharp fall of the collapse moment resistance for lengths between 4 and 8 m, also, it was observed that beams with low or intermediate $\overline{\lambda}_{LT}$ had experienced VM for A, LTB + VM for B, or VM + WPB for D. The LTB failure mode becomes the dominant failure and occurs at intermediate and high $\overline{\lambda}_{LT}$, for E, C, F, Fig. 12 (b). Similarly, to the observation made for ambient, the higher the ratio H/h, the higher the collapse moment resistance at elevated temperature. For the beam with L = 5 m labelled B, at the temperature of 500 °C, the LTB + VM failure mode took place instead of VM at 20 °C.
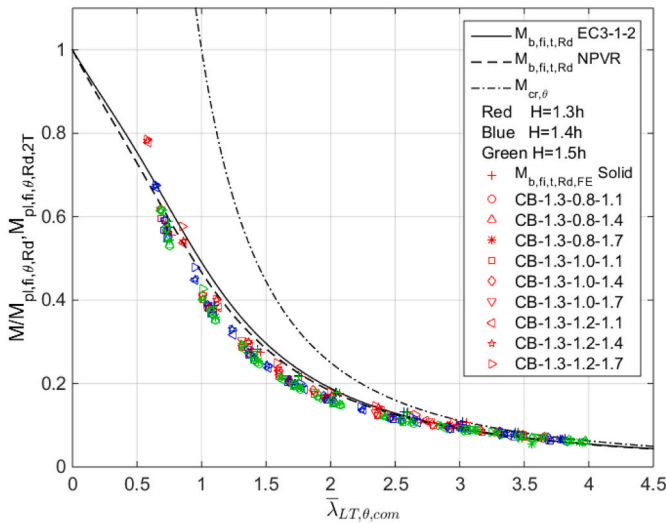
The average difference between numerical and analytical results for CB cases involving LTB failure modes or combinations of LTB with other
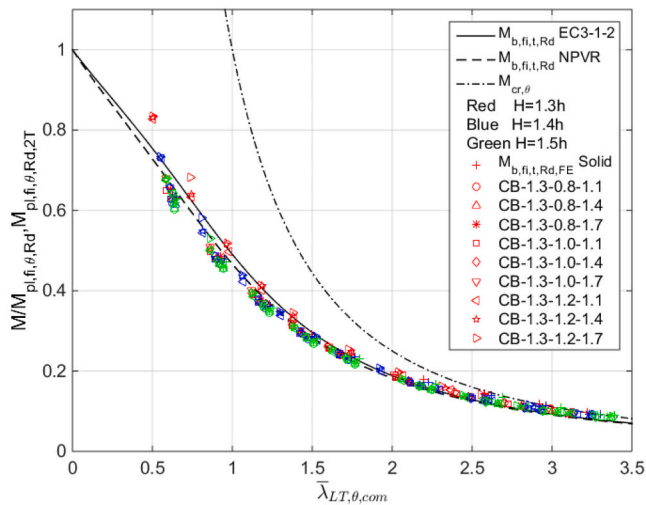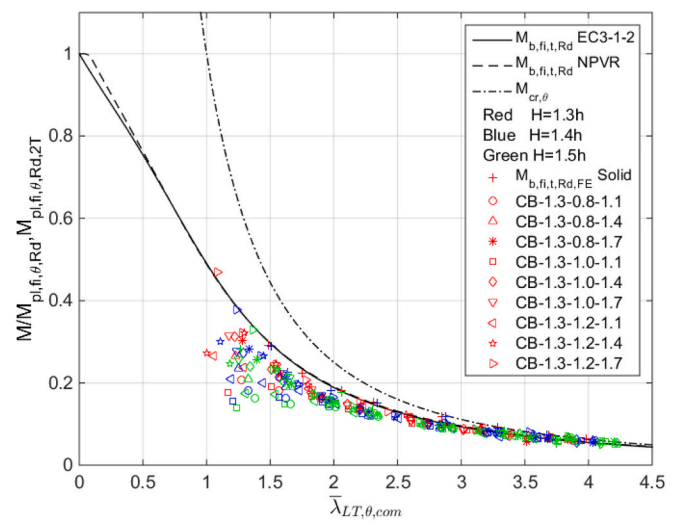
(a) End moment, θ=500°C
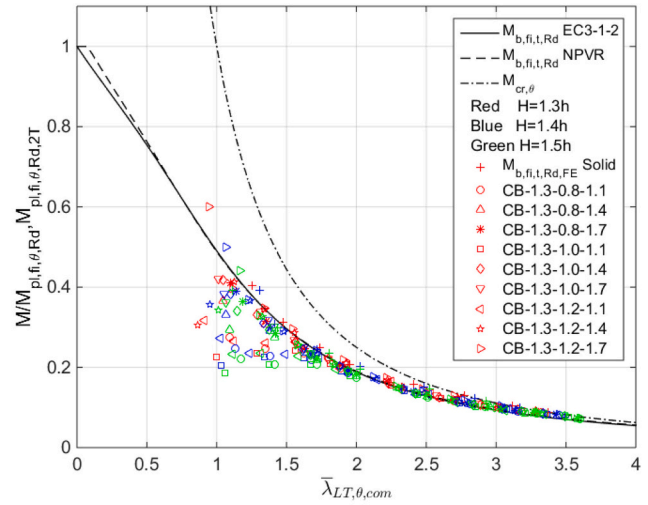
(b) Distributed load, θ=500°C

(c) End moment, θ=700°C

(d) Distributed load, θ=700°C

Fig. 11. Comparison between numerical and analytical reduction factors for LTB against non-dimensional slenderness (a-b) at θ = 500 °C, (c-d) at θ = 700 °C.

local modes approached 10% and 13% at 500 °C and 700 °C, respectively.

8. Development of a new plateau length of the LTB curves for cellular beams

The parametric study and the analysis presented in Section 7.2, for cellular beams subjected to a uniformly distributed load at ambient temperature have revealed that there are significant disparities between numerical and actual LTB design curves provided by EC3–1–1 §§ 6.3.2.2 [13]. These disparities were found to fall within the "non-conservative" side of the ($\overline{\lambda}_{LT}$, $M/M_{pl,Rd}$, $M_{pl,Rd,2T}$) plane, pointing to local failure modes and resulting in numerical moment resistances lower than those of code values. These were observed more frequently for "beams with small or intermediate slenderness", but disparities were small for those with high slenderness, which sets the points closer to the buckling curve "b". Numerical results showed also that when using EC3 curves, the actual critical behaviour of a particular section is not adequately represented because most of the properties of the cellular beam sections are based solely on the depth-to-width ratio h/b, particularly in beam cases with ratios S/a_0 indicating narrow web posts or ratios a_0/h indicating

large openings.

When confronting the numerical LTB resistance curves with the Eurocode buckling curve, it becomes clear that there is a need to increase the consistency of the latter. This is only possible by setting a new plateau length of the LTB curves based on cellular beam geometric parameters. Lower values of the numerically normalized moment resistance giving rise to local failure and couple modes were disregarded, and the study focuses on the LTB failure mode only.

This proposal considers the statistical method of mean squared error (MSE), to predict a new plateau length of the LTB curves for simply supported cellular beams under uniformly distributed load. The input data required for the model are the key parameters of the cellular beam cross-section (H/h, a_0/h, and S/a_0) and the beam slenderness.

A new equation was worked out based on the MATLAB Curve Fitting App using the Poly21 surface-fitting model. A numerical database for beam parameters together with non-dimensional slenderness, Table 8, is used and the FE results chosen are within the limits of 0 to 10% above the buckling curve. It is important to point out that, an improvement of data within the limit in the range of 0 to 10 were adopted, considering two new cases, $a_0/h = 1.0$, $S/a_0 = 1.1$, and $a_0/h = 1.2$, $S/a_0 = 1.4$, for L = 7 m.
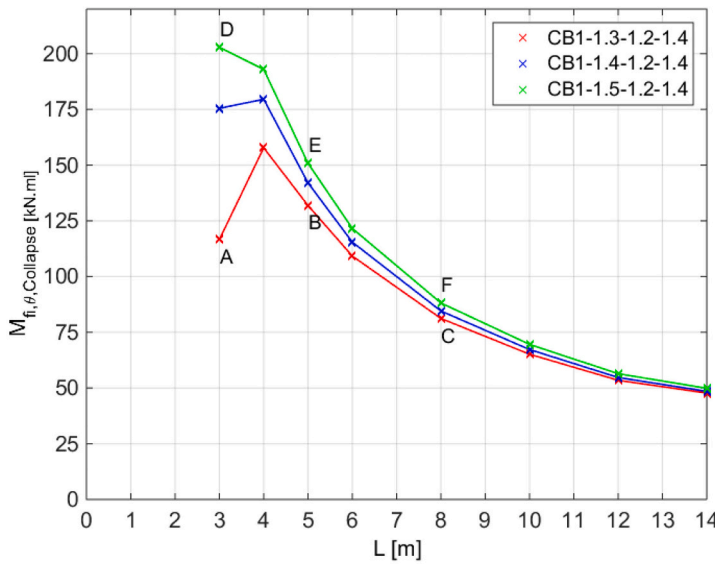
Table 6
Summary of the failure modes related to the investigated cases at θ = 500 °C.

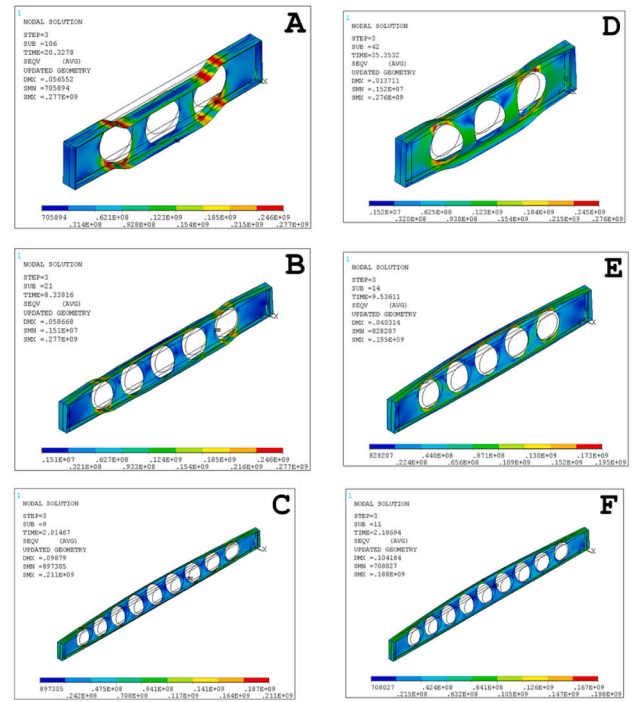| Case 1 (θ = 500 °C)	L (m)	$\bar{\lambda}_{LT,0,FE}$	Failure mode	Case 2	L (m)	$\bar{\lambda}_{LT,0,FE}$	Failure mode	Case 3	L (m)	$\bar{\lambda}_{LT,0,FE}$	Failure mode
CB-1.3-0.8-1.1	3–5	1.09–1.62	WPB	CB-1.4-0.8-1.1	3–4	1.13–1.38	WPB	CB-1.5-0.8-1.1	3–4	1.18–1.41	WPB
	6	1.88	LTB+		5	1.67	LTB + WPB		5	1.71	LTB + WPB
	8–14	2.33–3.33	LTB		6–14	1.94–3.45	LTB		6	2.00	LTB+
									8–14	2.51–3.60	LTB
CB-1.3-0.8-1.4	3	1.04	WPB	CB-1.4-0.8-1.4	3	1.07	WPB	CB-1.5-0.8-1.4	3	1.09	WPB
	4	1.35	LTB + WPB		4	1.38	LTB + WPB		4	1.41	LTB + WPB
	5	1.62-	LTB+		5–14	1.67–3.44	LTB		5–14	1.72–3.59	LTB
	6–14	1.88–3.28	LTB								
CB-1.3-0.8-1.7	3	1.1	LTB + WPB	CB-1.4-0.8-1.7	3–4	1.14–1.39	LTB+	CB-1.5-0.8-1.7	3	1.19	LTB + WPB
	4–14	1.35–3.29	LTB		5–14	1.68–3.43	LTB		4	1.42	LTB+
									5–14	1.72–3.58	LTB
CB-1.3–1.0-1.1	3–5	1.00–1.56	WPB	CB-1.4-1.0-1.1	3–5	1.03–1.62	WPB	CB-1.5-1.0-1.1	3–5	1.06–1.67	WPB
	6	1.81	LTB + WPB		6	1.89	LTB+		6	1.95	LTB+
	8–14	2.24–3.18	LTB		8–14	2.35–3.37	LTB		8–14	2.44–3.52	LTB
CB-1.3–1.0-1.4	3–4	1.05–1.29	LTBWPB+VM	CB-1.4-1.0-1.4	3	1.1	WPB	CB-1.5-1.0-1.4	3	1.15	WPB
	5	1.56	LTB+		4	1.34	LTB + WPB		4	1.37	LTB + WPB
	6–14	1.80–3.16	LTB		5	1.62	LTB+		5	1.67	LTB+
					6–14	1.88–3.34	LTB		6–14	1.94–3.49	LTB
CB-1.3–1.0-1.7	3	1.01	LTB + WPB + VM	CB-1.4-1.0-1.7	3	1.06	WPB	CB-1.5-1.0-1.7	3	1.07	WPB
	4	1.31	LTB+		4	1.37	LTB+		4–14	1.41–3.49	LTB
	5–14	1.56–3.14	LTB		5–14	1.62–3.33	LTB				
CB-1.3–1.2-1.1	3–5	0.91–1.35	WPB + VM	CB-1.4-1.2-1.1	3–5	1.02–1.49	WPB	CB-1.5-1.2-1.1	3–5	1.11–1.58	WPB
	6	1.57	WPB+		6	1.73	LTB + WPB		6	1.85	LTB + WPB
	8–14	1.93–2.75	LTB		8–14	2.15–3.09	LTB		8–14	2.31–3.34	LTB
CB-1.3–1.2-1.4	3	0.87	VM	CB-1.4-1.2-1.4	3	0.95	VM	CB-1.5-1.2-1.4	3	1.01	WPB + VM
	4–5	1.12–1.34	LTB + VM		4	1.24	LTB+		4	1.33	LTB+
	6	1.55	LTB+		5–14	1.48–3.06	LTB		5–14	1.58–3.32	LTB
	8–14	1.92–2.73	LTB								
CB-1.3–1.2-1.7	3	0.94	LTB	CB-1.4-1.2-1.7	3	1.06	LTB	CB-1.5-1.2-1.7	3–4	1.17–1.31	LTB+
	4–5	1.11–1.34	VM/VM+		4	1.23	LTB + VM		5–14	1.58–3.30	LTB
	6	1.55	LTB+		5	1.47	LTB+				
	8–14	1.91–2.70	LTB		6–14	1.71–3.03	LTB				

Table 7
Summary of the failure modes related to the investigated cases at θ = 700 °C.

Case 1 (θ = 700 °C)	L (m)	$\lambda_{LT,0,FE}$	Failure mode	Case 2	L (m)	$\lambda_{LT,0,FE}$	Failure mode	Case 3	L (m)	$\lambda_{LT,0,FE}$	Failure mode
CB-1.3-0.8-1.1	3–5	1.28–1.90	WPB	CB-1.4-0.8-1.1	3–4	1.33–1.62	WPB	CB-1.5-0.8-1.1	3–4	1.37–1.66	WPB
	6–14	2.21–3.90	LTB		5	1.96	LTB + WPB		5	2.01	LTB + WPB
					6–14	2.28–4.04	LTB		6–14	2.35–4.22	LTB
CB-1.3-0.8-1.4	3	1.22	LTB + WPB	CB-1.4-0.8-1.4	3	1.25	WPB	CB-1.5-0.8-1.4	3	1.28	WPB
	4	1.58	LTB+		4	1.62	LTB+		4	1.66	LTB + WPB
	5–14	1.90–3.85	LTB		5–14	1.96–4.03	LTB		5–14	2.01–4.21	LTB
CB-1.3-0.8-1.7	3–4	1.29–1.59	LTB+	CB-1.4-0.8-1.7	3	1.34	LTB + WPB	CB-1.5-0.8-1.7	3	1.39	LTB + WPB
	5–14	1.91–3.84	LTB		4–14	1.63–4.02	LTB		4–14	1.67–4.20	LTB
CB-1.3–1.0-1.1	3–4	1.17–1.51	WPB	CB-1.4-1.0-1.1	3–4	1.21–1.57	WPB	CB-1.5-1.0-1.1	3–4	1.24–1.61	WPB
	5	1.82	LTB + WPB		5	1.91	LTB + WPB		5	1.96	LTB + WPB
	6–14	2.12–3.72	LTB		6	2.22	LTB+		6–14	2.29–4.13	LTB
					8–14	2.75–3.95	LTB				
CB-1.3–1.0-1.4	3	1.22	LTB + WPB	CB-1.4-1.0-1.4	3	1.29	LTB + WPB	CB-1.5-1.0-1.4	3	1.34	WPB
	4	1.51	LTB+		4–14	1.57–3.91	LTB		4	1.61	LTB+
	5–14	1.82–3.69	LTB						5–14	1.96–4.10	LTB
CB-1.3–1.0-1.7	3	1.18	LTB + WPB	CB-1.4-1.0-1.7	3	1.24	LTB + WPB	CB-1.5-1.0-1.7	3	1.25	LTB + WPB
	4–14	1.54–3.68	LTB		4–14	1.60–3.90	LTB		4–14	1.65–4.09	LTB
CB-1.3–1.2-1.1	3	1.24	WPB + VM	CB-1.4-1.2-1.1	3	1.19	WPB + VM	CB-1.5-1.2-1.1	3–4	1.30–1.54	WPB
	4	1.29	VM		4	1.44	WPB		5	1.85	LTB + WPB
	5	1.55	LTB + WPB + VM		5	1.73	LTB + WPB		6–14	2.16–3.91	LTB
	6–14	1.80–3.17	LTB+		6	2.02	LTB+				
					8–14	2.50–3.60	LTB				
CB-1.3–1.2-1.4	3	1.0	VM	CB-1.4-1.2-1.4	3	1.11	WPB + VM	CB-1.5-1.2-1.4	3	1.18	WPB + VM
	4	1.30	LTB + VM		5–14	1.45–3.57	LTB		4–14	1.55–3.89	LTB
	5	1.55	LTB+								
	6	1.79–3.15	LTB								
CB-1.3–1.2-1.7	3	1.09	LTB	CB-1.4-1.2-1.7	3–14	1.24–3.53	LTB	CB-1.5-1.2-1.7	3–14	1.36–3.85	LTB
	4	1.28	LTB + VM								
	5	1.54	LTB+								
	6–14	1.78–3.11	LTB								

Fig. 12. (a) LTB moment resistance versus cellular beam length at θ = 500 °C with H/h = 1.3, 1.4, and 1.5; a0/h = 1.2; S/a0 = 1.4. (b) Corresponding Von misses stress at failure for cellular beams with L of 3, 5, 8 m from left to right.

Table 8
Performance ratio between FE and predicted results for H/h = 1.3.

Model no.	H/h	S/a_0	a_0/h	$\bar{\lambda}_{LT,FE}$	$\bar{\lambda}_{LT,PV}$	Ratio (FE/PV)
1	1.3	1.1	0.8	1.65	1.61	1.02
2	1.3	1.1	1.0	1.79	1.74	1.03
3	1.3	1.1	1.2	1.85	1.86	1.00
4	1.3	1.4	0.8	1.18	1.25	0.94
5	1.3	1.4	1.0	1.37	1.45	0.94
6	1.3	1.4	1.2	1.67	1.65	1.01
7	1.3	1.7	0.8	0.96	0.88	1.08
8	1.3	1.7	1.0	1.15	1.17	0.99
9	1.3	1.7	1.2	1.48	1.45	1.02

A suitable equation that best fits the FE results is suggested to be used for predicting the slenderness limit for the LTB design of cellular beams. It can be expressed based on the ratios a_0/h and S/a_0 by the following function:

$$\bar{\lambda}_{LT,0} = 3.64 - 0.86*(a_0/h) - 2.28*(S/a_0) + 1.33*(a_0/h)*(S/a_0) \tag{11}$$

To check the validity and dependability of the suggested equation, its outcomes for the non-dimensional slenderness of the cellular beams were compared to the numerical database. The comparison were made in terms of the goodness-of-fit statistics for the polynomial fit (R^2) and the performance ratio ($\bar{\lambda}_{LT,FE}$ / $\bar{\lambda}_{LT,PV}$), where $\bar{\lambda}_{LT,FE}$ is the numerical value of non-dimensional slenderness, and $\bar{\lambda}_{LT,PV}$ is the value of the non-dimensional slenderness predicted from the fitting equation. Smith's research results [49] showed that a satisfactory state can be reached when the R^2 is >0.8 and the differences between the experienced and predicted values are smallest. We determined that, the coefficient of determination (R^2) of the surface was relatively close to 1.0 (0.9706), showing that the proposed equation was convenient. Furthermore, Table 8 shows the ratio of the FE results to the suggested equation ($\bar{\lambda}_{LT,FE}/\bar{\lambda}_{LT,PV}$), which had an average ratio of 1.01. A detailed analysis of

the results reveals that for >89% of the data, the difference between the parametric numerical results $\bar{\lambda}_{LT,FE}$ and the values predicted $\bar{\lambda}_{LT,PV}$ by the model equation was ±6. Consequently, all numerical results have been covered by the suggested equation.

The suggested modification to the EC3 buckling curve closely follows the actual European LTB design rules "general case", except for the use of the maximum value of $\bar{\lambda}_{LT,0}$. A further notable change was that the value of the modified reduction factor, $\chi_{LT,mod}$, becomes a variable that depends on $\bar{\lambda}_{LT,0}$ rather than the constant value 1.

Fig. 13 depicts the comparison of LTB analytical results predicted by Eurocode 3, $M_{b,Rd}$, and overall predicted LTB moment resistances of the proposed equation for $M_{b,Rd,PV}$, with the actual FE collapse moment resistance, $M_{Coll.Rd}$. Prediction error limits of ±10% is plotted with red symbols representing EC3 analytical results, and blue symbols representing theoretically predicted results.

Most of data points were within the conservative zone and the formulation was proved to meet the desired conditions and being able to better estimate the slenderness limit against the LTB design of the perforated beams compared to numerical results. On the other hand, for values $M_{Coll.\ Rd}/M_{pl,\ Rd,\ FE} \leq M_{b,\ Rd,\ NP}/M_{pl,\ Rd,\ 2T}$, odd points that tend towards the non-conservative zone are cases where the slenderness was less than the slenderness limit at which the LTB must be calculated. An example problem is considered in Appendix A, where this method is compared with the current Eurocode 3 design methodology.

9. Conclusion

The work presents a set of parametric studies to investigate the influence of cross-section height, opening size, web-post width, and non-dimensional slenderness on the LTB behaviour of cellular beams. A uniform bending and a distributed load were analysed at ambient and elevated temperatures, considering a nonlinear analysis with geometric and material imperfections. From the analysis results, the predominant failure modes and collapse moment resistance could be obtained for the
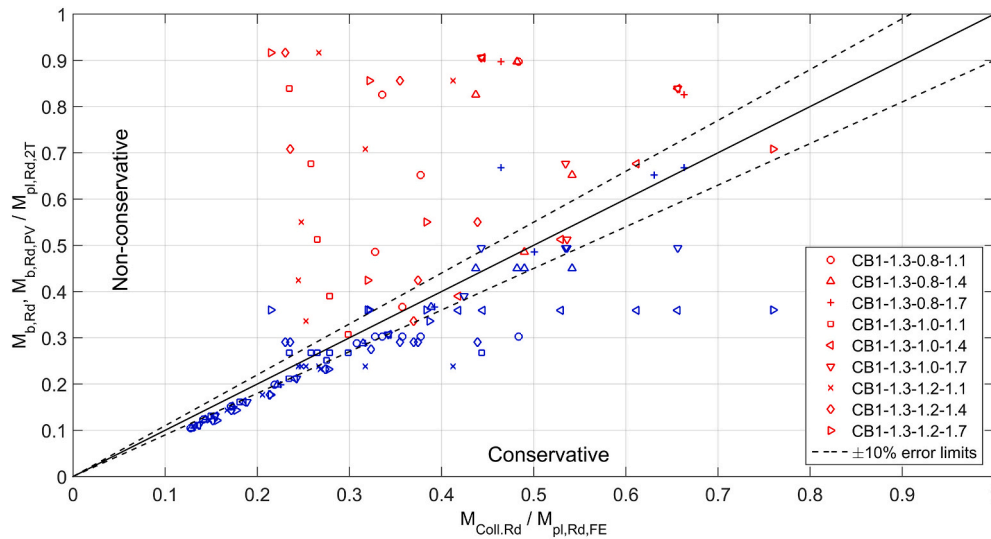
Fig. 13. Comparisons of numerical results, analytical results predicted by the Eurocode 3 (in red colour), and theoretical results predicted by the proposed equation (in blue colour). (For interpretation of the references to colour in this figure legend, the reader is referred to the web version of this article.)

studied cellular beams. The parametric numerical results have enabled to establish a fit equation to predict the plateau length of the LTB curves for cellular beams.

The following main conclusions can be set:

- The use of the numerical coupling during the elastic and buckling simulations, cancels the cross-section local buckling, and it allows to capture the LTB mode without being superimposed or combined with other buckling modes.
- For the case of uniform bending the predominant failure modes were LTB and LTB + P-2 T. However, for uniform distributed load, the failure modes vary with geometric parameters and generically with the CBs slenderness, noticing failure due to LTB, 2 T-section (P-2 T), bending of the Top tee section (B-1 T), web or web post-buckling (WB or WPB), and Vierendeel mechanism VM.
- The VM mechanism can occur when the perforated steel beam along the span has relatively large openings (a_0/h = 1.0, 1.2). A WPB failure mode may occur if the cellular beams have narrow web posts. For all web-post widths analysed with $\lambda_{LT} \leq 0.55$ and a_0/h = 0.8, 1.0, the interaction of shear and web buckling V + WB may occur. For a_0/h = 1.2, the failure due to bending of top tees section B-1 T is verified.
- Over the whole slenderness range of CBs subjected to distributed load, neither of the two LTB design curves, b, and c, provides accurate estimates of the cellular beam design resistance. Additional failure modes must be considered for short beams, which give design resistances smaller than both LTB design curves. For intermediate and high non-dimensional slenderness, the curve b from Eurocode 3 "general case" clause 6.3.2.2, using an equivalent solid beam, gives better predictions.
- At elevated temperatures, similar behaviour is obtained. Nevertheless, due to the loss of stiffness caused by increased temperature, the LTB becomes the dominant failure mechanism even for beams with smaller slenderness.
- On average the difference between numerical and the simplified design results for CB cases involving LTB failure modes or combinations of LTB with other modes, which includes intermediate and

high non-dimensional slenderness, approaches 13% at θ = 20 °C, 10% at θ = 500 °C, and approaches 13%. at θ = 700 °C.
- The proposed model for the new plateau length of the LTB curves for cellular beams allows a better prediction of the CBs behaviour against LTB. It considers the key geometric parameters of the perforated cross-section: H/h, a_0/h, and S/a_0. Nonetheless, additional verifications should be developed for other CBs with different height ratios.

In particular, the failure modes of web-post buckling and the Vierendeel collapse mechanism were not deeply addressed in this study, but further work is needed to define the CBs geometric dimensions and the slenderness threshold that changes the failure mechanisms allowing for a safe design against LTB.

CRediT authorship contribution statement

Sabrina Benyettou Oribi: Methodology, Software, Validation, Formal analysis, Writing – original draft. **Abdelhak Kada:** Methodology, Investigation, Writing – review & editing, Supervision. **Belkacem Lamri:** Methodology, Investigation, Writing – review & editing, Supervision. **Luis Mesquita:** Methodology, Investigation, Conceptualization, Writing – review & editing, Supervision.

Declaration of Competing Interest

None.

Data availability

Data will be made available on request.

Acknowledgments

Appendix A. Comparison of Eurocode and proposed method for LTB resistance of a cellular beam under distributed load

To compare the EC3 general method to the proposed method, the normalized design LTB resistance and numerical collapse resistance, $M/M_{pl,Rd,2T}$, for a cellular beam model under distributed load were plotted against the non-dimensional slenderness, $\bar{\lambda}_{LT}$, Fig. A14. Table A1 shows the cellular beam geometric parameters and the design results for comparison.

Table A1
Cellular beam design verification.

H/h	a_0/S	S/a_0	L (m)	$\lambda_{LT,EC3}$	$M_{b,Rd,EC3}$ (kN.m)	$M_{Coll.FE}$ (kN.m)	$\lambda_{LT,0}$ (Eq. (11))	$M_{b,Rd,NP}$ (kN.m)	$M_{b,Rd,EC3}$ / $M_{Coll.FE}$	$M_{b,Rd,NP}$ / $M_{Coll.FE}$
1.3	1.0	1.7	3	0.876	440.04	355.22	1.165	323.61	1.24	0.91

Table A1, shows that the EC3 general method overpredicts the LTB design moment in 1.24 times the FE moment resistance value. Applying Eq. (11), to determine the slenderness limit, this value is corrected to 0.91 giving a safe estimation of the LTB design resistance. This case is plotted in Fig. A14, where the FE result and the new plateau are represented together with the Eurocode design curves for comparison.
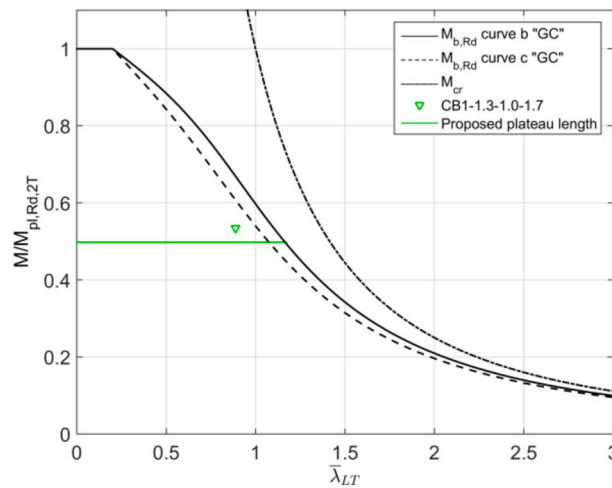
Fig. A14. Comparison between the proposed and the EC3 methods for a cellular beam with H/h = 1.3, a0/h = 1.0, S/a0 = 1.7.

References

[1] D. Kerdal, D.A. Nethercot, Failure modes for castellated beams, J. Constr. Steel Res. 4 (4) (1984) 295–315, https://doi.org/10.1016/0143-974X(84)90004-X.

[2] S. Demirdjian, Stability of Castellated Beam Webs, McGill University Montreal, Canada, 1999.

[3] K.F. Chung, T.C.H. Liu, A.C.H. Ko, Investigation on Vierendeel mechanism in steel beams with circular web openings, J. Constr. Steel Res. 57 (5) (2001) 467–490, https://doi.org/10.1016/S0143-974X(00)00035-3.

[4] F. Erdal, M.P. Saka, Ultimate load carrying capacity of optimally designed steel cellular beams, J. Constr. Steel Res. 80 (2013) 355–368, https://doi.org/10.1016/j.tws.2020.106955.

[5] P. Panedpojaman, T. Thepchatri, S. Limkatanyu, Novel design equations for shear strength of local web-post buckling in cellular beams, Thin-Walled Struct. 76 (2014) 92–104, https://doi.org/10.1016/j.tws.2013.11.007.

[6] F.P.V. Ferreira, R. Shamass, L.F.P. Santos, V. Limbachiya, K.D. Tsavdaridis, EC3 design of web-post buckling resistance for perforated steel beams with elliptically-based web openings, Thin-Walled Struct. 175 (2022), 109196, https://doi.org/10.1016/j.tws.2022.109196.

[7] J. Nseir, M. Lo, D. Sonck, H. Somja, O. Vassart, N. Boissonnade, Lateral torsional buckling of cellular steel beams, Proc. Ann. Stab. Conf. Struct. Stab. Res. Council (2012) 18–21.

[8] D. Sonck, Global Buckling of Castellated and Cellular Steel Beams and Columns, Ph. D Thesis,, Ghent University, 2014.

[9] D. Sonck, J. Belis, Lateral–torsional buckling resistance of cellular beams, J. Constr. Steel Res. 105 (2015) 119–128, https://doi.org/10.1016/j.jcsr.2014.11.003.

[10] P. Panedpojaman, W. Sae-Long, T. Chub-uppakarn, Cellular beam design for resistance to inelastic lateral–torsional buckling, Thin-Walled Struct. 99 (2016) 182–194, https://doi.org/10.1016/j.tws.2015.08.026.

[11] N. Boissonnade, J. Nseir, M. Lo, H. Somja, Design of cellular beams against lateral torsional buckling, Proc. Inst. Civ. Eng. Struct. Build. 167 (7) (2014) 436–444, https://doi.org/10.1680/stbu.12.00049.

[12] CEN, Draft-EN-1993-1-13, Eurocode 3 Part 1.13 Steel Beams with Large Web Openings, European Committee for Standardization, Brussels, Belgium, 2017.

[13] CEN, EN-1993-1-1, Eurocode 3: Design of Steel Structures - Part 1–1: General Rules and Rules for Buildings, European Committee for Standardization, Brussels, Belgium, 2005.

[14] F.P.V. Ferreira, A. Rossi, C.H. Martins, Lateral-torsional buckling of cellular beams according to the possible updating of EC3, J. Constr. Steel Res. 153 (2019) 222–242, https://doi.org/10.1016/j.jcsr.2018.10.011.

[15] K. Rajana, K.D. Tsavdaridis, E. Koltsakis, Elastic and inelastic buckling of steel cellular beams under strong-axis bending, Thin-Walled Struct. 156 (2020), 106955, https://doi.org/10.1016/j.tws.2020.106955.

[16] F.P.V. Ferreira, R. Shamass, V. Limbachiya, K.D. Tsavdaridis, C.H. Martins, Lateral–torsional buckling resistance prediction model for steel cellular beams generated by artificial neural networks (ANN), Thin-Walled Struct. 170 (2022), 108592, https://doi.org/10.1016/j.tws.2021.108592.

[17] M.E.A. Ben Seghier, H. Carvalho, C.C. de Faria, J.A.F.O. Correia, R.H. Fakury, Numerical analysis and prediction of lateral-torsional buckling resistance of cellular steel beams using FEM and least square support vector machine optimized by metaheuristic algorithms, Alexandr. Eng. J. 67 (2023) 489–502, https://doi.org/10.1016/j.aej.2022.12.062.

[18] CEN, EN-1993-1-2, Eurocode 3: Design of Steel Structures - Part 1–2: General Rules - Structural Fire Design, European Committee for Standardization, Brussels, Belgium, 2005.

[19] C. Bailey, Indicative fire tests to investigate the behaviour of cellular beams protected with intumescent coatings, Fire Saf. J. 39 (8) (2004) 689–709, https://doi.org/10.1016/j.firesaf.2004.06.007.

[20] L.M.R. Mesquita, P.A.G. Piloto, M.A.P. Vaz, P.M.M. Vila Real, Experimental and numerical research on the critical temperature of laterally unrestrained steel I beams, J. Constr. Steel Res. 61 (10) (2005) 1435–1446, https://doi.org/10.1016/j.jcsr.2005.04.003.

[21] A. Nadjai, O. Vassart, F. Ali, D. Talamona, A. Allam, M. Hawes, Performance of cellular composite floor beams at elevated temperatures, Fire Saf. J. 42 (6–7) (2007) 489–497.

[22] O. Vassart, A. Bouchair, J.P. Muzeau, A. Nadjai, Analytical model for the web post buckling in cellular beams under fire, 2008, pp. 3–11. https://www.researchgate.net/publication/273122182.

[23] E. Ellobody, B. Young, Behaviour of composite frames with castellated steel beams at elevated temperatures, Adv. Struct. Eng. 19 (7) (2016) 1060–1076, https://doi.org/10.1177/1369433216631620.

[24] L. Mesquita, J. Gonçalves, G. Gonçalves, P. Piloto, K. Abdelhak, Intumescente fire protection of cellular beams, in: X Congresso de Construção Metálica e Mista, Coimbra, Portugal, 2015, pp. 623–630. http://hdl.handle.net/10198/12482.

[25] B. Lamri, L. Mesquita, K. Abdelhak, P. Piloto, Behavior of cellular beams protected with intumescent coatings, Fire Res. 1 (1) (2017) 27–32, https://doi.org/10.4081/fire.2017.27.

[26] P. Wang, X. Wang, M. Liu, L. Zhang, Web-post buckling of fully and partially protected cellular steel beams at elevated temperatures in a fire, Thin-Walled Struct. 98 (2016) 29–38, https://doi.org/10.1016/j.tws.2015.02.028.

[27] A. Nadjai, K. Petrou, S. Han, F. Ali, Performance of unprotected and protected cellular beams in fire conditions, Constr. Build. Mater. 105 (2016) 579–588, https://doi.org/10.1016/j.conbuildmat.2015.12.150.

[28] CEN/TC2503, prEN-1993–1-2, Eurocode 3: Design of Steel Structures - Part 1–2: General Rules - Structural Fire Design, European Committee for Standardization, Brussels, Belgium, 2018.

[29] O. Vassart, M. Hawes, I. Simms, B. Zhao, J.-M. Franssen, A. Nadjai, Fire resistance of long span cellular beam made of rolled profiles (FICEB), Bruxelles, Belgique (2012), https://doi.org/10.2777/38158.

[30] S. Benyettou Oribi, A. Kada, B. Lamri, L.M.R. Mesquita, Numerical analysis of lateral torsional buckling of steel I-beams with and without web-openings under fire, in: 5th Iberian-Latin-American Congress on Fire Safety _ 5 CILASCI, Porto, Portugal, 2019, p. 10.

[31] J. Silva, P. Dalcanal, L. Mesquita, Numerical analysis of cellular steel beams failure modes in fire conditions, in: P.A.G. Piloto, J.P. Rodrigues, V.P. Silva (Eds.), Advances in Fire Safety Engineering. CILASCI 2019, Lecture Notes in Civil Engineering, Springer, Cham, 2020, pp. 78–92, https://doi.org/10.1007/978-3-030-36240-9_6.

[32] S. Benyettou Oribi, A. Kada, B. Lamri, L.M. Mesquita, Investigation of residual stresses on the fire resistance of unrestrained cellular beams, Ce/Papers 4 (2–4) (2021) 1386–1394, https://doi.org/10.1002/cepa.1436.

[33] C. Correa de Faria, H. Carvalho, R. Hallal Fakury, L. Figueiredo Grilo, Lateral-torsional buckling resistance of cellular steel beams at room temperature and fire situation, Eng. Struct. 237 (2021), 112046, https://doi.org/10.1016/j.engstruct.2021.112046.

[34] A. Kada, B. Lamri, L. Mesquita, A. Bouchair, Finite element analysis of steel beams with web apertures under fire condition, Asian, J. Civ. Eng. 17 (2016) 1035–1054.

[35] ANSYS®, ANSYS® Mechanical APDL Product Launcher 2022 R2, 2022.

[36] R. Lawson, S. Hicks, Design of composite beams with large web openings, in: Accordance with Eurocodes and the UK National Annexes, Steel Construction Institute, 2011, https://doi.org/10.13140/RG.2.2.19276.62085.

[37] J. Valeš, T.-C. Stan, FEM modelling of lateral-torsional buckling using shell and solid elements, Procedia Eng. 190 (2017) 464–471, https://doi.org/10.1016/j.proeng.2017.05.365.

[38] C. Martins, F. Ferreira, A. Rossi, E. Trentini, Numerical analysis of physical and geometrical imperfections in cellular beams, Open J. Civ. Eng. 07 (2017) 116–129, https://doi.org/10.4236/ojce.2017.71007.

[39] A. Rossi, D. Hideyuki Saito, C. Humberto Martins, A. Sander Clemente de Souza, The influence of structural imperfections on the LTB strength of I-beams, Structures 29 (2021) 1173–1186, https://doi.org/10.1016/j.istruc.2020.11.020.

[40] F. Teixeira, R. Caldas, L. Grilo, Influence of different shapes of geometric imperfections on the structural behavior of beams with large web openings, ISSN 1816-112X, 2020, p. 272, https://doi.org/10.18057/IJASC.2020.16.3.8.

[41] N. Boissonnade, H. Somja, Influence of imperfections in FEM modeling of lateral torsional buckling, in: Proceedings of the Annual Stability Conference, Structural Stability Research Council Grapevine, Texas, 2012, pp. 1–15.

[42] N. Rossini, M. Dassisti, K. Benyounis, A.-G. Olabi, Methods of measuring residual stresses in components, Mater. Des. 35 (2012) 572–588, https://doi.org/10.1016/j.matdes.2011.08.022.

[43] M. Abambres, W.-M. Quach, Residual stresses in steel members: a review of available analytical expressions, Int. J. Struct. Integrity 7 (1) (2016) 70–94, https://doi.org/10.1108/IJSI-12-2014-0070.

[44] P. Panedpojaman, T. Thepchatri, S. Limkatanyu, Novel simplified equations for Vierendeel design of beams with (elongated) circular openings, J. Constr. Steel Res. 112 (2015) 10–21, https://doi.org/10.1016/j.jcsr.2015.04.007.

[45] N. Boissonnade, R. Greiner, J.-P. Jaspart, J. Lindner, Rules for Member Stability in EN 1993-1-1; Background Documentation and Design Guidelines, European Convention for Constructional Steelwork. http://www.steelconstruct.com/site/#, 2006.

[46] P.M.M. Vila Real, N. Lopes, L. Simões da Silva, J.M. Franssen, Parametric analysis of the lateral–torsional buckling resistance of steel beams in case of fire, Fire Saf. J. 42 (6) (2007) 416–424, https://doi.org/10.1016/j.firesaf.2006.11.010.

[47] A.C.S, S.A, ACB® and Angelina® beams - A new generation of beams with large web openings, in: ArcelorMittal (Ed.), 2021, p. 64.

[48] D.L. Kennedy, M.A. Hafez, A study of end plate connections for steel beams, Can. J. Civ. Eng. 11 (2) (1984) 139–149, https://doi.org/10.1139/l84-026.

[49] G.N. Smith, Probability and Statistics in Civil Engineering - an Introduction, Collins professional and technical books, London, 1986.